UNIVERSITÀ DEGLI STUDI DI PADOVA

DIPARTIMENTO DI INGEGNERIA DELL'INFORMAZIONE

DIPARTIMENTO DI INGEGNERIA DELL'INFORMAZIONE

CORSO DI LAUREA IN BIOINGEGNERIA

INTEGRATION OF MICROFLUIDICS, SENSING, AND DATA PROCESSING FOR AUTOMATED BIOLOGICAL ASSAYS

Relatore: Prof. Alessandro Paccagnella

Tutor esterno: Ing. Francesco Ferrara

Correlatore: Prof. Stefano Bonaldo

Laureando: Alfredo De Cillis

ANNO ACCADEMICO 2023 – 2024

Data di laurea: 16 Ottobre 2024

SUMMARY

FIGURE INDEX

PREFACE

This thesis work arises from my internship period spent at the Institute of Nanotechnology of Consiglio Nazionale delle Ricerche (CNR NANOTEC) in Lecce, conducted from November 2023 to July 2024.

CNR NANOTEC Institute in Lecce is a multidisciplinary center for research and development in nanotechnologies. The center's activities focus on innovative models and approaches of nanotechnology in different domains, ranging from fundamental research to the development of cutting-edge technologies, including applied projects that address both industrial needs and societal challenges. Scientific and experimental activities are carried out within national and international projects and collaborations with academic and industrial partners and can be classified into four core thematic platforms: Materials, Photonics and Optoelectronics, Nanobiotechnology, and Advanced Devices [1]. The center is supported by an extensive infrastructure of laboratories organized in seven facilities. These facilities support a wide range of activities including the synthesis and advanced characterization of new materials, device fabrication, functional systems, and devices. [1]

The research activities of CNR Nanotec in Lecce focus on the following main areas of interest:

- Advanced Devices
- Materials Science
- Modeling & Computation
- Nano-Biotechnology
- Photonics & Optoelectronics
- PlasmaCheM [1]

During my internship period, I had the opportunity to work within a heterogeneous research group, which allowed me to interact with people specialized in research fields different from mine but united by the achievement of the same goal. Therefore, I also had the opportunity to enhance my engineering knowledge, particularly at the software/hardware level, which was available to the group and as support to their research activities. The primary activity I performed is presented in this thesis. In the following pages, I will not only report the work I performed but I will also describe my experience over the past months.

Figure 1. CNR NANOTEC in LECCE, Campus Unisalento

ABSTRACT

The development of an electrochemical biosensor capable of detecting concentrations of target molecules from a biological sample is often complex, time consuming, and requires a high degree of selectivity and affordability. This challenge is particularly significant when only a limited number of devices and samples are available for testing. This work presents a tool that automates and controls an integrated system comprising electrochemical measurement system, a microfluidics platform, and post-processing. A proof-of-concept application of this system is demonstrated through the development of a pesticide detection platform.

A typical sequence of operations to perform the realization of this detection system might include an electro-deposition phase to form binding sites for the molecule of interest usually followed by multiple washing steps and incubation steps before the test can be conducted on the device. These steps require several hours of manual work, resulting in a very time-consuming process in which manual control could introduce high variability and errors. By automating the entire process, the system allows users to simply configure the list of operations, which the platform then performs autonomously.

The system also supports conducting large number of electrochemical measurements in series and of different types, displaying them in different ways, and finally allows the user to classify, organize automatically, and possibly process the result. This simplifies the work for the user by reducing workload and minimize potential human errors.

The resulting system has been applied to a real case study, involving the detection of *cyromazine*, a pesticide used in the agri-food industry. If unchecked, *cyromazine* can pose health risks, including kidney damage highlighting the importance of precise and reliable detection.

1. CHAPTER 1: BACKGROUND

1.1. ELECTROCHEMISTRY PRINCIPLES

The oxidation-reduction reaction (REDOX) is a chemical reaction in which the oxidation number of chemical species that participate changes. Examples of REDOX reaction can be the rusting of metals or the browning of fruit. This reaction is formed by two half-reaction, an oxidation e a reduction in which a net chemical change is involved, i.e. an atom or electron is transferred from an element of the reaction to another.

REDOX reactions are classified according to the element being transferred, and this element can be:

- An Oxygen-atom, in which an atom of Oxygen is transferred from the reduced species to the oxidized species
- A Hydrogen-atom, in which an atom of Hydrogen is transferred from the oxidized species to the reduced species
- An Electron, in which electrons are transferred from the oxidized species to the reduced species [2]

Focusing on the electrons transfer reaction, an oxidation semi-reaction is accompanied by the formation of positive ions, instead electrons are gained in a reduction semi-reaction. Reaction in which both processes happen are called REDOX reactions [3].

To better understand this phenomenon the voltaic cell example is presented below.

A voltaic cell is composed by two half-cells, each of these has an electrode in aqueous solution containing ions. Half of the redox reaction occurs at each half cell. When the two half cells are connected together with a wire and a salt bridge, they form an electrochemical cell. In Figure 2 is presented a schematic of a typical voltaic cell [4].

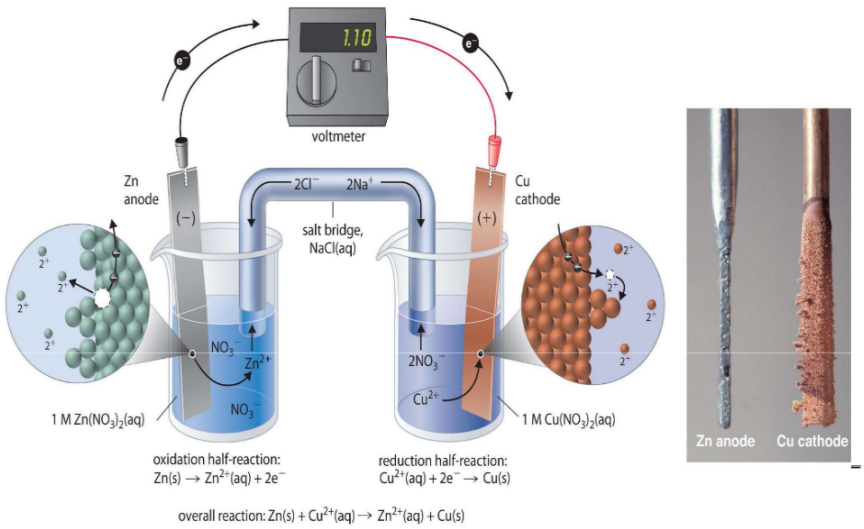

Figure 2. The Reaction of Metallic Zinc with Aqueous Copper(II) Ions in a Galvanic Cell (left), result on both electrodes of the REDOX reaction. [3]

Voltaic cell in Figure 2 is constructed by inserting a copper electrode into a recipient that contains an aqueous 1 M solution of Cu^{2+} ions (right) and a zinc electrode into a different recipient that contains an aqueous 1 M solution of Zn^{2+} ions (left). The two electrodes are connected by a voltmeter and the wires are connected to the two electrodes so that the current can flow. The recipients are connected by a salt bridge, a U-shaped tube inserted into both solutions that contains a saline solution (NaCl(aq)). When the circuit is closed, in the left half cell the zinc electrode (the anode) is spontaneously oxidized to Zn^{2+} ions, while Cu^{2+} ions are simultaneously reduced to copper metal at the copper electrode (the cathode). As the reaction progresses, the Zn anode loses mass as it dissolves to give Zn^{2+}(aq) ions, while the Cu cathode gains mass as Cu^{2+}(aq) ions are reduced to copper metal that is deposited on the cathode. The oxidative and reductive half-reactions are physically separated from each other. The electrons that are released at the anode flow through the wire, producing an electric current. Galvanic cells therefore transform chemical energy into electrical energy that can then be used to produce work. [3].

The electrolyte in the salt bridge is used to complete the circuit by carrying electrical charge and maintains electrical neutrality in both solutions by allowing ions to migrate between them.

The potential (*Ecell*) of the cell, measured in volts, is the difference between the electric potential of the two half cells. In the cell we have described, the voltmeter indicates a potential of 1.10 V [3].

Electrochemical redox conversion between ferricyanide and ferrocyanide on a gold or platinum electrode is one of the most classical reactions in electrochemistry.

Ferricyanide, $Fe(CN)_6^{3-}$, is an iron containing complex that can easily undergo redox reactions. In aqueous solution it can be reduced (gain an electron) to ferrocyanide (reduction reaction):

$$Fe(CN)_6^{3-} + e^- \rightarrow Fe(CN)_6^{4-}$$

While the oxidation is:

$$Fe(CN)_6^{4-} + e^- \rightarrow Fe(CN)_6^{3-}$$

Tracking electron transfer processes at electrode–electrolyte interfaces is of great significance for a wide range of applications from bioanalytical chemistry to material science. $[Fe(CN)_6]^{3/4}$ has long been used as a standard electroactive probe in the investigation of the electron transfer capabilities of various electrode materials. Owing to its facile modification, gold has become one of the most frequently used electrode materials. [5]

The gold electrode is seen as chemically inert, on which only the adsorption/desorption of $[Fe(CN)_6]^{3/4-}$ and electron transfer take place [5] (Figure 3).

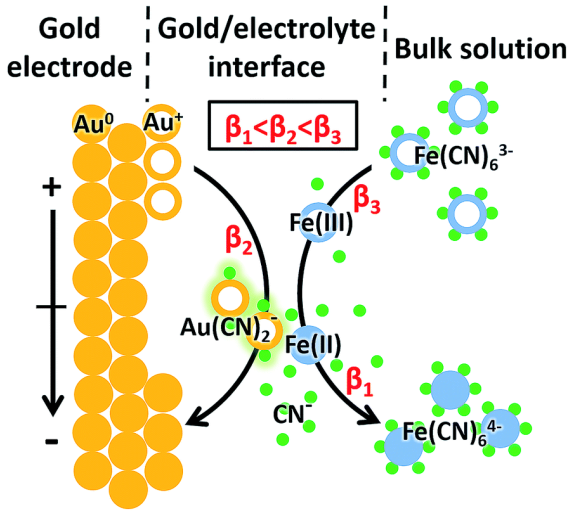

Figure 3. Proposed mechanism of the interaction between $[Fe(CN)_6]^{3/4-}$ and the gold electrode. β_1, β_2 and β_3 represent the cumulative formation constants for $Fe(CN)_6^{4-}$, $Au(CN)_2^-$ and $Fe(CN)_6^{3-}$, respectively [5].

The gold electrode participates in the redox reaction of $[Fe(CN)_6]^{3/4-}$ by competing with it to form $Au(CN)_2^-$, since the formation constant is $Fe(CN)_6^{3-} > Au(CN)_2^- > Fe(CN)_6^{4-}$. The formation rate of $Au(CN)_2^-$ depends on the ratio of Fe(III) and Fe(II) on the surface of the gold electrode, which is determined by the redox conversion between Fe(III) and Fe(II) thus by the electric field force-

based attraction or repulsion between the gold electrode and $[Fe(CN)_6]^{3/4-}$. This factor is potential-dependent, resulting in the periodic change of $Au(CN)_2^-$ in the dynamic potential scan of $[Fe(CN)_6]^{3/4-}$. [5]

Electroanalytical chemistry is the branch of chemistry that uses electrochemical methods to obtain information related to concentration and characteristics of chemical species. In these techniques, an electrode probe is used for the qualitative and the quantitative analysis of compounds under investigation. The chemical properties of these compounds are related to the potential of the cell. Being the potential of the electrode controllable, this method is highly selective so it's possible to determine the electrochemical spectrum of electroactive species in the solution [6].

In voltammetry, while varying the potential in a selected range, the current is measured, and this is related to information about an analyte of interest like its concentration in the solution. The potential E varied arbitrarily step by step or continuously and the actual current value is measured as the dependent variable. The potential is varied to cause oxidation or reduction of electroactive species at the electrode. The resultant current is proportional to the concentration of the electrochemical species. The commonly employed voltametric techniques are Cyclic Voltammetry and Differential Pulse Voltammetry [6].

1.2. ELECTROCHEMICAL CHARACTERIZATION TECHNIQUES

1.2.1. CYCLIC VOLTAMMETRY

Cyclic voltammetry is the most widely used electroanalytical technique for acquiring qualitative information about electrochemical reactivity. It's useful for the study of interfacial processes and soluble reaction intermediates. In Cyclic Voltammetry, the current response of small stationary microelectrode is recorded as a function of a ramp in potential [6].

A typical electrode configuration is shown in Figure 4.

It's a three electrodes configuration in which the Potential of the ramp ΔE is applied between the Working electrode and the Reference electrode while the current is measured between the Reference electrode and the Counter electrode. Working and Counter electrodes are made of the same material, platinum or gold, while the Reference is in silver in a solution of silver chloride.

A two-electrodes configuration also exists, in which there is only a Working and a Reference electrode. The Potential is applied between the two electrodes and in the same two the current is measured. This configuration is not recommended for measurements in which large potential variations are involved [7].

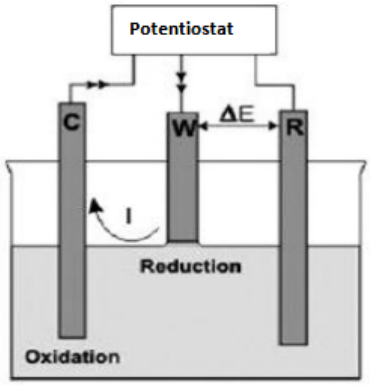

Figure 4. Three electrodes configuration. Left: The working (W) and the counter (C) are made of the same material, i.e. platinum or gold while the Reference (R) is in Ag/AgCl. The ramp potential is applied between the electrodes of W and R while the current is measured between the electrodes of R and W [7]

The Potential applied has a sawtooth shape with Potential that varies between an upper and lower limit (Figure 5 Left)

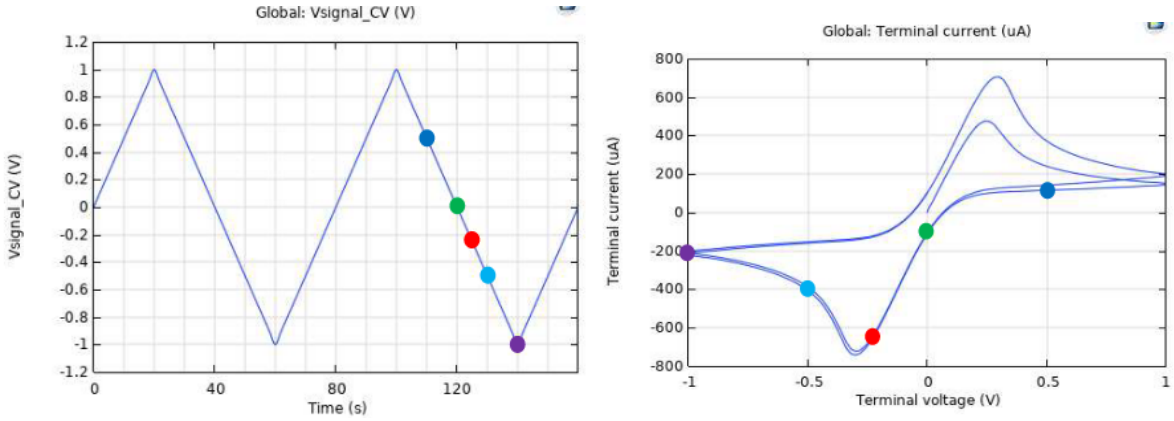

Figure 5. Left: Example of cyclic voltammetry scans at various timepoints (in blue 100 s, green 120 s, red 125 s, cyan 130 s, purple 140 s). Upper Vertex Potential = 1V, Lower Vertex Potential = -1V [7]. Right: Example of a voltammogram obtained using the potential ramp described in Figure 5. (in blue 100 s, green 120 s, red 125 s, cyan 130 s, purple 140 s). Upper Vertex Potential = 1V, Lower Vertex Potential = -1V [7].

The scan rate is calculated as

$$v = \frac{V_2 - V_1}{t_2 - t_1}$$

and defines the slope of the ramp, i.e. the velocity at which the potential reaches its maximum or minimum value. This is a critical value because the duration of a scan must provide sufficient time to allow the Oxidized species to be reduced properly or vice versa.

The course of the curve can be described as follows.

Starting from a time of 100 s, the value of the potential is at its maximum value, there will then be a downward ramp. In the first time points (approx. 110 s), there is no significant increase in the absolute value of the current, this is before the reduction potential of the oxidized species is reached.

At 120 s, the reduction process begins, although very slowly, the concentration of the oxidized species in contact with the electrode surface begins to decrease in favor of the concentration of the reduced species, meanwhile the absolute value of the current begins to increase.

At 125 s, the potential value is low enough for the reduction reaction to become particularly fast and the peak current value is approached. At this point, the concentration of oxidized species near the electrode surface is zero because it has all been reduced. For successive time points, therefore, even if the potential decreases, the current value can no longer increase, so it will decrease again until the minimum voltage value is reached.

The changes in the concentration of the oxidized species (Figure 6) and the reduced species (Figure 7) at the previously identified timepoints are presented.

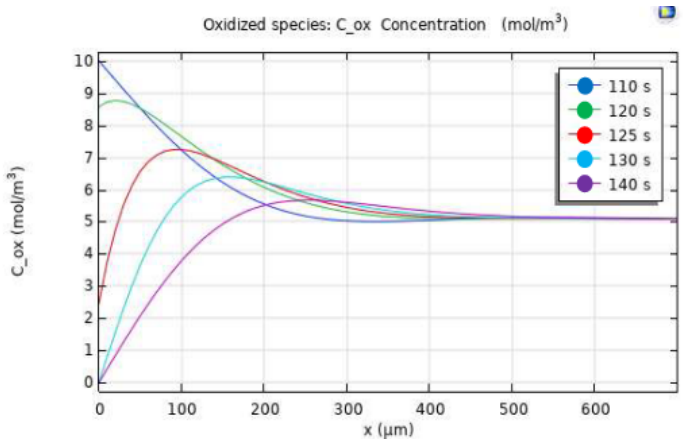

Figure 6. Variation of the Oxidized species during reduction semi-reaction at various timepoints [7].

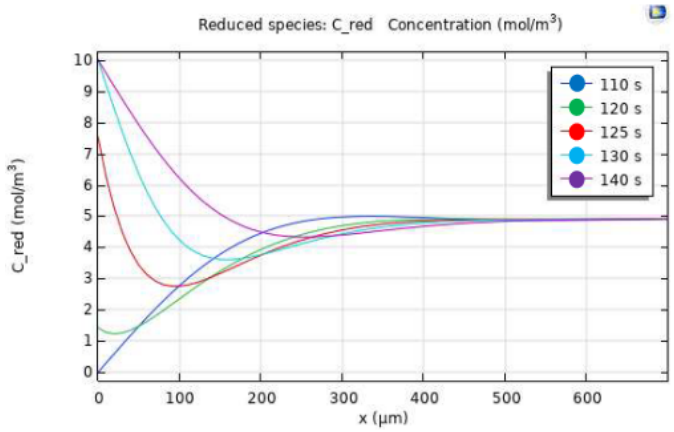

Figure 7. Variation of the Oxidized species during reduction semi-reaction at various timepoints [7].

The net cell current is given by the algebraic sum of the cathodic current (reduction) and anodic current (oxidation):

$$i_{net} = i_c + i_a$$

With:

$$i_c = nFAk_f^0 C_{ox} \exp\left(-\alpha nF \frac{E - E_q}{RT}\right)$$

$$i_a = nFAk_b^0 C_R \exp\left(-(1-\alpha)nF \frac{E - E_q}{RT}\right)$$

E_q is the reduction equilibrium potential, k_f^0 and k_b^0 are the forward (reduction) and backward (oxidation) rate constants of the redox reaction, α is the charge transfer coefficient (a positive

symmetry factor < 1), A is the working electrode area, and C_{ox} and C_R are the [Ox] and [Red] concentrations, respectively [7].

In Cyclic Voltammetry the information regarding an analyte concentration can be derived from the Peak Current and its position on the Potential axis (the Peak Voltage).

As mentioned earlier, current growth does not increase indefinitely, but once the peak is reached, it will decrease. This phenomenon is due to the fact that the concentration of oxidized [reduced] species near the electrode surface decreases due to the reduction [oxidation] process. The current is therefore limited by the diffusion rate from the bulk of the solution and not by the diffusion of electrons. This is defined by Fick's first law:

$$-J = \frac{dN}{dt} = D\ \frac{dC}{dt}$$

$$i_d = nFAD\frac{dC}{dt}$$

Where N is the number of moles, C the concentration, t the time, x the distance to the electrode, D the diffusion coefficient.

The potential at which the peak occurs, E_p, is correlated to the standard reduction potential E_0

$$E_p = E_0 + 0.059\frac{V}{2n}$$

The reversibility of a redox process is verified by the following conditions:

- $\frac{|i_{pa}|}{i_{pc}} = 1$; i.e. the ratio between anodic and cathodic peak current is 1
- $\Delta E = 0.059\frac{V}{2n} - \left(-0.059\frac{V}{2n}\right) = 0.059\frac{V}{n}$; where n is the number of electrons transferred
- $i_p = cost\ (v)^{1/2}$; the current peak intensity should be proportional to the square root of the scan rate (v)

In a reversible electron-transfer situation, the peak current (i_p) is given by the Randles-Sevcik equation (in this case for cathodic peak):

$$i_p = cost\ nFAC_{OX}(\frac{nFvD}{RT})^{1/2} = 2.686\ x\ 10^5\ n^{3/2}\ A\ D^{\frac{1}{2}}\ C_{OX}\ v^{1/2}\ A$$

In an irreversible process, peak will move away from each other between each cycles. In this case the Randles-Sevcik equation (for cathodic peak) is:

$$i_p = 2.98\ x\ 10^5\ n\ (\alpha\ n_a\ )^{1/2}\ AD^{1/2}\ C_{OX}\ v^{1/2}\ A$$

The reversibility of a redox process does not depend only on the redox molecules but also on the experimental conditions, such as the electrode material (like gold or platinum).

1.2.2. DIFFERENTIAL PULSE VOLTAMMETRY

Differential pulse voltammetry (DPV) is a pulse technique commonly used for the analysis of compounds, that involves applying amplitude potential pulses (10-100 mV) on a linear ramp potential. In DPV, a base potential value, chosen at which there is no faradaic reaction and applied to the electrode is increased between pulses with equal increments. The current is immediately measured before the pulse application (base current) and at the end of the pulse (pulse current), and the difference between them is recorded giving the DPV signal [8] . The difference between the measured currents and applied potentials results in a graph and the curve recorded is called differential pulse voltammogram. The height of each peak current recorded during the analysis is directly proportional to the concentration of the corresponding analyte and gives qualitative and quantitative information about it.

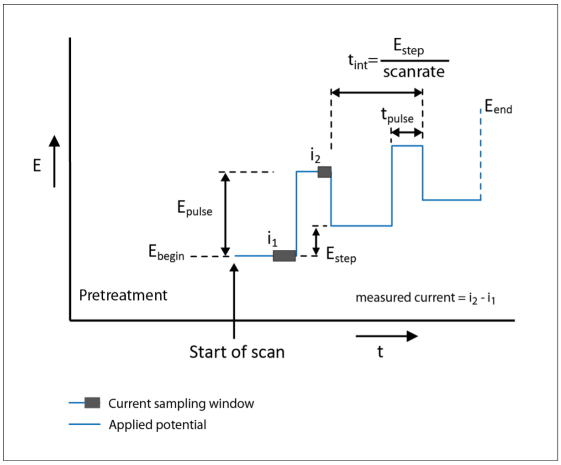

Figure 8. Schematics of a DPV scan. At each step the resulting current is calculated as the difference between the current obtained after the pulse and the current calculated before the pulse.

Like in Cyclic Voltammetry with linear sweep, in DPV a peak in current can be observed for a given redox process (Figure 9). In the linear sweep technique the qualitative information of an analyte is given by the Peak Current and Peak Voltage in the voltammogram. Similarly, in DPV, the peak potential, *Ep* and the peak current *ip,* are identified. The DPV is therefore a graph of differences between measured currents and applied potentials [8].

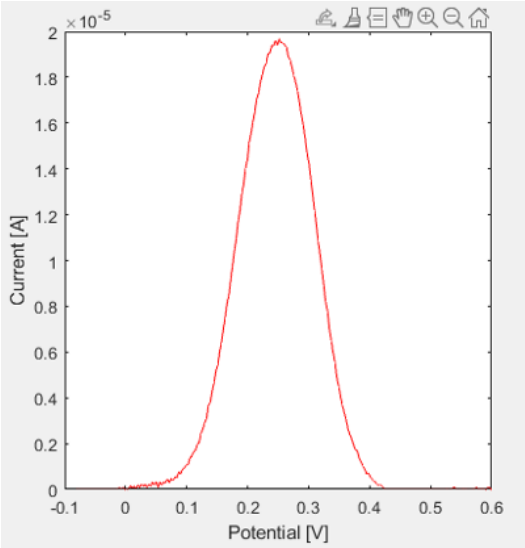

Figure 9. Example of a DPV curve. On x-axes the Potential Applied on y-axes the Current

In general, pulse techniques, such as DPV, are more sensitive than the linear sweep methods because there is minimization of the capacitive current. In turn, CV is most commonly used for exploratory purposes. Thus, in general, in sensor development both techniques are used, indeed CV provides essential information, such as the process reversibility, stability and types of redox processes in the analysis, whereas the pulse techniques are used for quantitative determinations, i.e. peak potential and current [8].

1.3. ELECTROCHEMICAL BIOSENSORS

In recent years, the focus on point-of-care methods has increased significantly, and with it, advances in the development of electrochemical biosensors. Electrochemical biosensors, which convert biological information into easily processed electrical signals, have been extensively explored for various bio-applications since they are sensitive, specific, inexpensive, easy to miniaturize and capable of detecting analytes in real time, thus resulting suitable for point-of-care

diagnostics. In addition, the continuous response of the electrochemical sensor enables computerized control, simplifying electrochemical detection and further reducing costs and analysis time. [9]

Electrochemical sensing techniques mainly use enzymes, due to their specific binding capacity and biocatalytic activity. Also, the use of capture probes like antibodies, aptamers or single strand nucleic acids is very common in the development of biosensing tools.

In (bio-) electrochemistry, the reaction under investigation may generate: (a) a measurable current between the electrodes, in the case of amperometric sensors; (b) a measurable potential or charge build-up between the electrodes, in the case of potentiometric sensors; or (c) may alter the conductive properties of a medium between the electrodes, in the case of conductivity sensors; another type of electrochemical sensing technique is impedance measurement (both resistance and reactance). Since reactions are generally only detected near the electrode surface, the electrodes themselves play a crucial role in the performance of electrochemical biosensors: in fact, the electrode's material, the modification of its surface and its size greatly influence its detection capability.

Electrochemical sensing usually requires a reference electrode, a counter electrode or auxiliary electrode and a working electrode, also known as a sensing or redox electrode.

The reference electrode, commonly made of Ag/AgCl, is kept at a distance from the reaction site to maintain a known, stable potential; the working electrode acts as a transduction element in the biochemical reaction, while the counter electrode establishes a connection to the electrolyte solution so that a current can be applied to the working electrode. These electrodes must be both conductive and chemically stable; therefore, compounds made of platinum, gold, carbon (e.g. graphite) and silicon are commonly used, depending on the analyte of interest. [10]

An example of the most common electrochemical sensors is represented by amperometric devices, which continuously measure the current resulting from the oxidation or reduction of an electroactive species.

The Clark oxygen electrode is the simplest form of amperometric biosensor: in this case, the intensity of the produced current is proportional to the oxygen concentration, which is measured by the reduction of oxygen on a platinum working electrode, with reference to a Ag/AgCl reference

electrode placed at a given potential. Generally, the current is measured at a constant potential and, in this case, this is an example of amperometry.

In voltammetry, on the other hand, the electric current inside an electrochemical cell is measured as the potential difference imposed at the ends of the cell changes. From such measurements, it is possible to determine the nature and quantity of an (electroactive) analyte: in fact, the potential at which the current peak occurs provides a qualitative indication of the chemical species to be determined, while the intensity of the current provides a quantitative figure, being proportional to the concentration of the species in solution. Since not all protein analytes are intrinsically capable of acting as redox partners in electrochemical reactions, these devices use mediators on the working electrode. [10]

1.4. CASE OF STUDY: DETECTION OF PESTICIDES IN THE AGRI-FOOD SECTOR

1.4.1. INTRODUCTION TO THE STUDY

Cyromazine is a highly selective insecticide with strong systemic and stomach poisoning abilities and is widely used in the agri-food sector in the cultivation of fruit and vegetables. In recent years, its excessive use has made it necessary to establish an accurate, fast and convenient method for the detection of this substance to ensure the safety of agricultural products. *Cyromazine* itself is not harmful to the human body, but its breakdown product, melamine, when ingested in large quantities could cause kidneys problems. Currently, the detection of *cyromazine* residues in food is mostly based on chromatographic techniques and ELISA kits, but they have several shortcomings such as the high equipment cost and long response time. For this reason, it is necessary to develop a detection method that is as accurate as possible and as fast as possible. In this sense, MIP-based devices sensors can overcome the limitations of the traditional detection methods mentioned above. [11]

1.4.2. MIP BIOSENSORS

Molecularly Imprinted Polymers (MIPs) are synthetic receptors that are complementary in size and shape to template molecules and can be used for the specific target purpose of molecule identification. Molecular imprinting is a process where the target molecule acts as a template around which interacting and cross-linking monomers are arranged and copolymerized to form a cast-like shell. Initially, the monomers form a complex with the template through covalent or non-covalent interactions. After polymerization and removal of the template, binding sites are exposed and are complementary to the target molecule in size, shape, and position of the functional groups, which are held in place by the cross-linked polymer matrix. In essence, a molecular memory is imprinted in the polymer, which is now capable of selectively rebinding the target molecule. The high specificity and stability of MIPs make them promising alternatives to enzymes, antibodies and other natural receptors used in sensor technologies. In fact, MIPs can offer greater long-term storage stability, low-cost production, potential reusability, resistance to microbial spoilage and custom synthesis of selective receptors, as well as facile integration with transducers. [12]

Moreover, molecules such as amino acids, nucleic acids and cholesterol increase the passage of current through polymer membranes after their binding has occurred. Therefore, MIPs are particularly suitable for applications in electrochemical sensors.

In principle, MIPs can be prepared for any analyte of interest, in fact synthetic receptors have been created for more than 10 000 biological molecules and structures, including inorganic ions, drugs, nucleic acids, proteins, viruses and even entire cells. The progress made in recent years in the field of MIP-based sensors has enabled a significant increase in their sensitivity, as it is possible to detect pico- and femto-molar concentrations of analyte [13]; moreover, research has now shifted towards the development of these sensors for real-life applications and POCTs performed on human samples.

Recently, electrochemical sensors based on MIPs have been developed using microparticles, nanoparticles or nanostructured coatings; one example is nanocarbon structures, such as graphene, which has special mechanical and electrical properties, as well as being biocompatible, easy and cheap to produce. In this case, the detection mechanism is based on conduction through nanochannels.

For example, a MIP for Adenine is made by forming a three-dimensional conductive layer following polymerisation. This manufacturing method increased the sensitivity and selectivity of the sensor for adenine, with a detection limit of approximately 1 nM [14] (Figure 10).

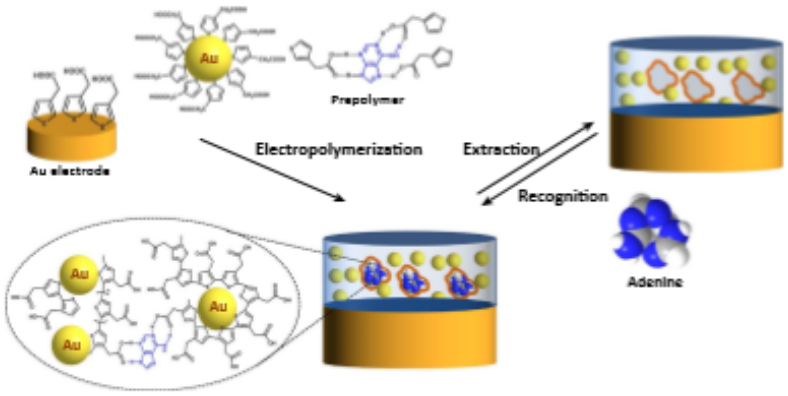

Figure 10. Fabrication of an adenine sensor based on MIP and three-dimensional conductive network [14]

Redox markers have been used in combination with MIP for the indirect detection of analytes in solution; in fact, the binding of the analyte with a MIP-coated electrode reduces the permeability of redox markers such as ferricyanide or ferrocene and this effect can be used to measure the analyte concentration.

Morphological changes in the polymer itself can occur as a result of specific interactions, leading to changes in the diffusion rate of the redox probe, which can be recorded as a change in the Faradic current (i.e. the current that develops at the electrode-electrolyte interface) [14].

The polymerization reaction is a complex process that depends on many factors such as the type and concentration of monomer, cross-linker and initiator, the temperature and polymerization time, the presence or absence of magnetic fields, and the volume of the polymerization solution. Therefore, the synthesis of a MIP is a complex process that involves the optimization of a wide variety of factors, first of all the choice of appropriate reagents. In general, the template molecule should meet certain requirements: it should not contain groups that take part in the polymerization reaction or hinder it; it should be extremely stable during the synthesis phase; and it should contain functional groups that are suitable for interacting with the monomer. Among the compounds that have attracted the most attention in recent years are drugs, antibiotics, anti-inflammatory agents, beta-blockers, due to their massive release into the environment, their effects on human health and their possible consequences in favoring the selection of drug-resistant pathogens [14].

1.4.3. CARBON BASED NANOTUBES COMPOSITE

Carbon Nanotubes effectiveness lies in the fact that they have good electrical properties and excellent mechanical strength. Because of their complementary electrical, electrochemical and mechanical properties, conductive polymers and Carbon Nanotubes (CNTs), if combined, may offer improved performances in supercapacitors. Electrochemical polymerization has no need for added oxidant and electrodeposited conductive polymers are naturally integrated as a continuous uniform film on the electrode [15]. The electrochemical co-deposition of CNTs with (poly)pyrrole in aqueous solution has been proven to be viable for the formation of these type of composites [15].

The electrochemical synthetized composite film of conducting polymer (poly)pyrrole (in our case) and CNTs have in common a porous structure at the micro- and nano- meter scales (Figure 11). They have better mechanical integrity, higher electronic and ionic conductivity, larger electrode specific capacitance and greater stability in charge-discharge cycles if compared with pure conducting polymers as seen in Figure 12 [15]. Specifically the capacitance of (poly)pyrrole-Carbon Nanotubes is doubled if compared to its only polymer counterpart [15].

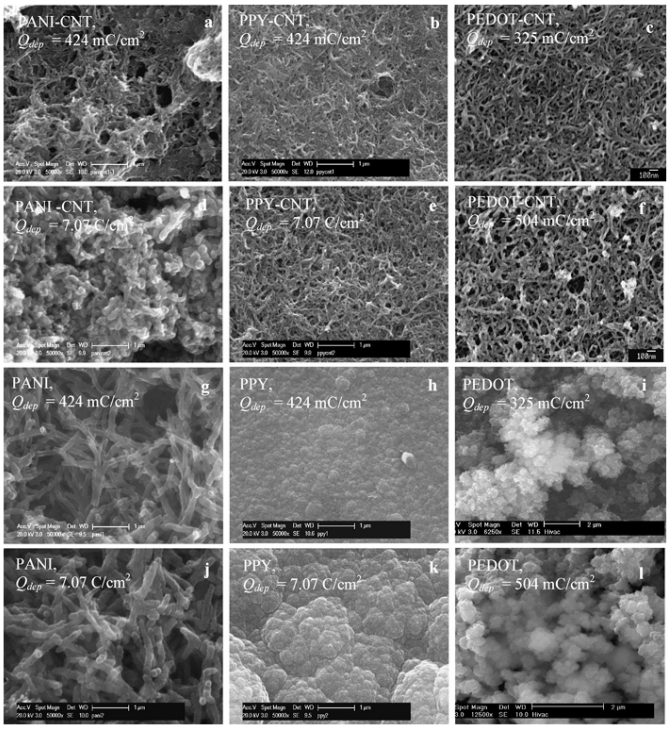

Figure 11. SEM images of the surfaces of CNTs composite film with polyaniline (PANI), (poly)pyrrole (PPY) and poly[3,4-ethylenedioxythiophene] (PEDOT) in figures a-j and their pure polymer counterparts in figures g-l [15].

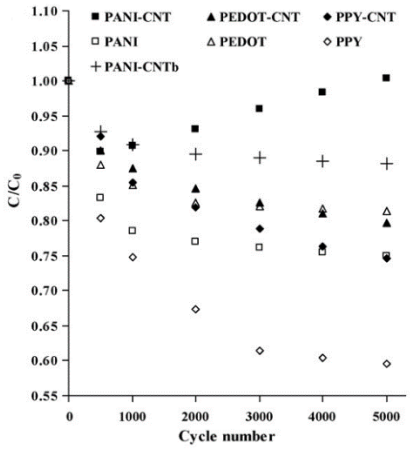

Figure 12. Plot capacitance shift against charge-discharge cycle number. Scan rate: 100 mV/s [15]

1.5. LABVIEW, AN OVERVIEW

LabVIEW (Laboratory Virtual Instrumentation Engineering Workbench) is the integrated development environment for National Instruments' visual programming language. The syntax in LabVIEW is not written but graphical, and for this reason it is called G-Language (Graphic Language).

Originally made for Apple Macintosh in 1986, LabVIEW is mainly used for programs for data acquisition and analysis, process control, report generation, or more generally for anything related to industrial automation, on various platforms such as Windows, Linux, macOS, and National Instruments controllers [16].

A program in LabVIEW, called VI (Virtual Instrument), does not exist in text form, but can only be saved as a binary file that can be opened and compiled only by the software [16].

The VI takes the form of a flowchart in which objects are connected by wires, each object has a specific function. This type of language is called dataflow because the sequence of execution is defined and represented by the flow of the data itself through the one-way wires connecting the functional blocks. Since data can also flow in parallel through non-consecutive blocks and threads, the language can spontaneously realize multithreading without the need for explicit programmer management [16].

LabVIEW programs are compatible with many models of programmable instruments and acquisition boards [16].

FRONT PANEL

The front panel is the user interface of the VI. It is realized with controls and indicators, which are the interactive input and output terminals, respectively. Controls are arrays, knobs, potentiometers, buttons, dials, and many others; they simulate instrument input devices and provide data to the block diagram of the VI. Indicators are graphs, tables, LEDs, thermometers, and many others; they simulate the output devices of instruments and display the data that the block diagram acquires or generates [16] (Figure 13 left).

BLOCK SCHEME

The block diagram is the flowchart representing the source code, in graphical format. Front panel objects appear as input or output terminals in the block diagram. Block diagram objects include:

- terminals
- functions
- constants
- structures
- calls to other VIs (subVIs)
- connecting threads
- textual comments

Functions are themselves VIs, although they do not have their own front panel and block diagram. They can have any number of inputs and outputs like any VI [16].

Structures perform basic flow control. For example, the FOR loop is represented by a rectangle that repeats N times the portion of the block diagram that is inserted inside it [16].

Link threads can carry theoretically any amount of data of any type, even programmer-defined aggregates (bundles). The wires can be of different thickness and color to allow easy identification of the data flowing through them: for example, whole numbers flow on blue wires, decimal numbers on orange wires strings on pink wires [16] (Figure 13 right).

The block diagram can also be made visible during execution, which is very useful in debugging, since there is the possibility of visualizing with a slow-motion animation the movement of data along the wires and its momentary value [16].

Each VI can itself be used as a subVI and appear within the block diagram of other VIs as any function, and as such can have inputs and outputs to which flow lines can be connected. A connector box is used to define input and outputs of the subVI, thus the appearance shown in the main VI. Typically, with a few clicks, each control can be associated with an input and each indicator can be associated with an output [16].

Stand-alone executables and shared libraries (DLLs) can also be created from VIs, because LabVIEW is a true 32-bit compiler [16].

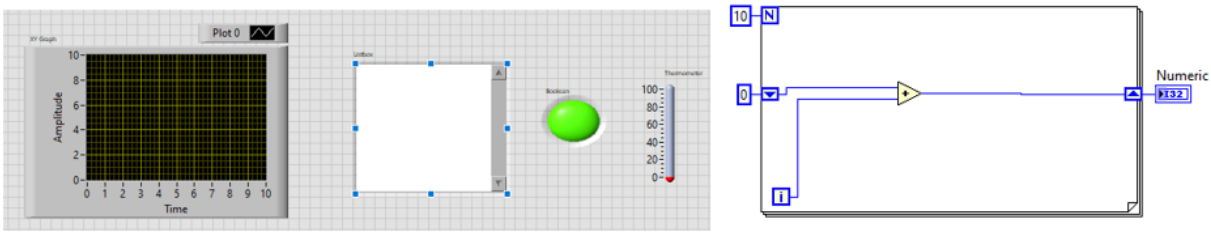

Figure 13. Left: From left to right: a Graph, a Table, a Led and a Thermometer. Right: A for loop with 10 repetitions in which using a numeric wire the sum of the ith element and the previous element is calculated and put in Numeric

2. CHAPTER 2: MATERIALS AND METHODS

2.1. OVERVIEW

The chapter has been divided into three macro-sections:

- Microfluidics control: all controls concerning the microfluidics system and liquid flowing functions;
- Autolab Control: involved managing the Autolab instrument to allow performing the electrochemical measurements;
- Post-processing: consists of saving measurements, organizing folders, calculating baseline and peak and area of curves.

I have designed these three areas separately but with the aim of being able to combine them into one system and control them simultaneously. The NI LabVIEW software [17] therefore serves as an ideal development environment because it simplifies hardware integration for engineering applications [17]. This makes it possible to integrate the Autolab control system, microfluidics and post-processing (post measurement) operations into a single application.

As can be seen in the following paragraphs, the application is designed to have a sequential control of the series of operations to be performed in order to obtain all the necessary steps for functionalization, washing and measurements. These operations indeed, include flow of liquids and cyclic voltammetry or differential pulse voltammetry measurements. Once the sequence of commands has been started, the application moves on to a section in which it can be seen the execution process of the various commands, the progress bar of liquid delivery, the measurements taken and other information such as the various measurement parameters. Finally, there is a post-processing section that will start as soon as the application has finished executing the last command in the sequence. In this section, a sequence of the measurements curves can be displayed and the baseline fit can be calculated and saved.

An application developed in this way allows the complete control over the entire system and guarantees all the advantages that an automated system brings.

A traditional measurement method in fact has very long idle times when it comes to measurement setup, measurement, post-processing and data organization. These limitations lead to a reduced number of measures, and therefore a reduced number of experiments.

This is why sequential processing of this kind, requiring no user intervention, allows for faster processing. The measurement setup is arranged to act automatically, as is the measuring and saving part. As a result, more measurements can be taken in series and more data can be stored.

Even in post-processing, the automation can guarantee an objective and systematic method for each measurement to calculate the baseline and thus the peak and area of a curve. The aim in these cases is to allow as few parameters as possible while still guaranteeing a certain level of robustness.

In conclusion, such a hardware system is designed with the aim of bringing together several components that can be described as ‘non-particularly complex’ to create a larger device that can be considered complex as a whole. A clear separation of the various parts also allows targeted intervention on the individual components, thus ensuring a high degree of flexibility with respect to the program being realized. For example, a modification to one of the three systems would require the exclusive intervention on the part of interest, so it is possible to guarantee a hardware system that can be easily updated and customized according to the user's needs. The development environment in LabVIEW allows this type of approach. I also paid attention to the costs and space occupied by the various components, keeping them as low as possible. The final idea is therefore to realize a large device that can be used in a research laboratory and thus take advantage of the high accuracy of this area while looking towards the speed and automation of the industrial system.

2.2. MICROPUMPS CONTROL

The micropump control system is designed for immediate liquid flushing without having to move or relocate the measurement setup. Four micropumps each connected to a different liquid then are employed for flushing, deposition, incubation and placement of the ferricyanide drop.

Overall, the entire system is small enough to ensure easy setup of the measurement environment, which is in line with the idea of making a hardware-friendly product, possibly keeping costs down as well.

2.2.1. GENERAL ELECTRONICS OF THE SYSTEM

For the development of this section I could rely on four Bartels Mikrotechnik mp6 micropumps. As I have already mentioned these are piezoelectric pumps whose operation is illustrated in Figure 14. [18]

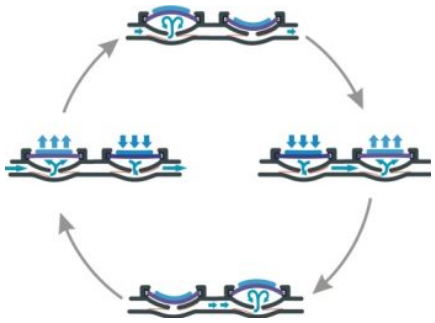

Figure 14 [18]. Operating cycle of the micropumps. The flow is regulated by the contraction/relaxation of the two diaphragms.

These micropumps feature a diaphragm in combination with two valves. When a tension is applied, the diaphragm contracts allowing the liquid to move. The opening/closing of the valves defines the direction of flow [18].

The four micropumps can be controlled simultaneously by connecting them to a QuadKey mp6, which is linked to a QuadOEM board. This board includes a microcontroller with command register for controlling the micropumps, as shown in Figure 15.

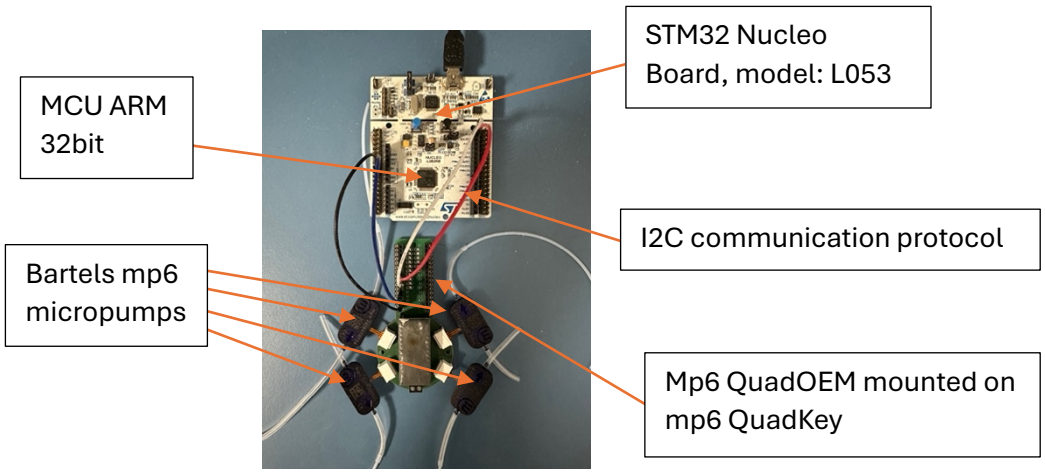

Figure 15. Connection of all elements that form the micropump control system

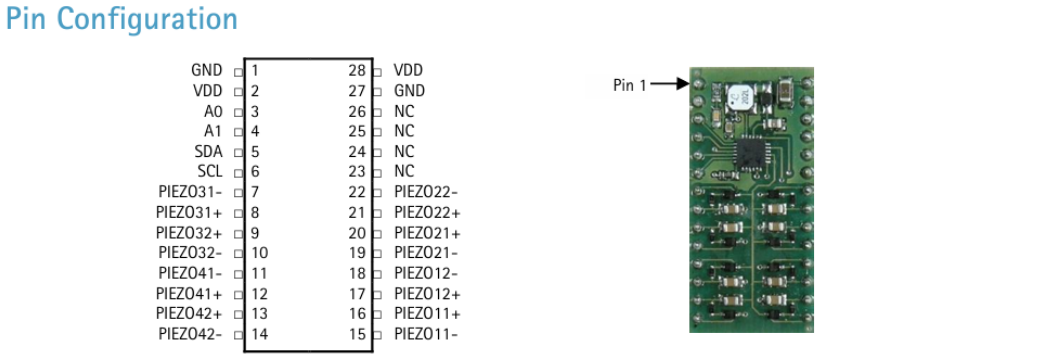

Figure 16. On the right the QuadOEM placed on the QuadKEY (covered by a gray paste in the first picture). While on the left we have the PIN diagram. [3]

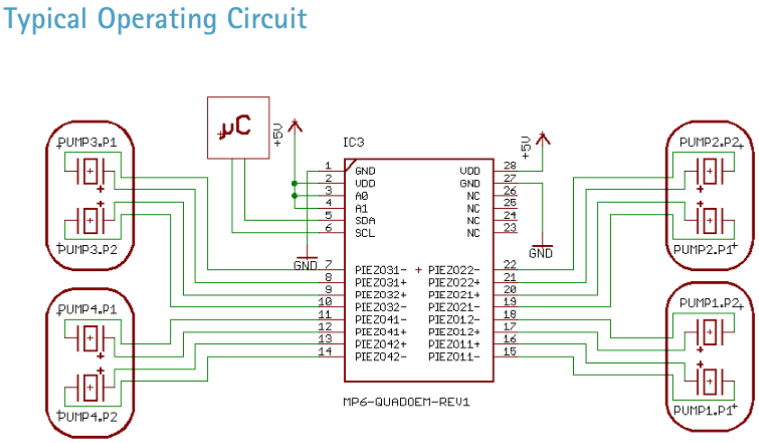

Figure 17. PIN schematics on [19] QuadKEY. [20]

The system is controlled using an Arduino Nano board. Communication between the Arduino board and the QuadOEM board is carried out through I2C protocol. The protocol, devised by Philips [19], allows communication between two devices using a bus consisting of two lines, SCL (serial clock line) and SDA (serial data line), where SCL takes care of communication synchronization (the clock) while SDA takes care of data transport. Communication is carried out through a master-slave system, where the master sends the address to the slave, which in turn takes care of receiving and transmitting. Figure 18 shows how the protocol works. The master begins transmission by carrying the signal from high to low. One bit of data will be transferred in each high-to-low cycle of the SCL signal. A change in SDA when SCL is still high is considered as a control signal. Specifically, START and REPEATED START CONDITION correspond to a change in SDA from high to low while SCL is high, while STOP corresponds to a change in SDA from low to high [20].

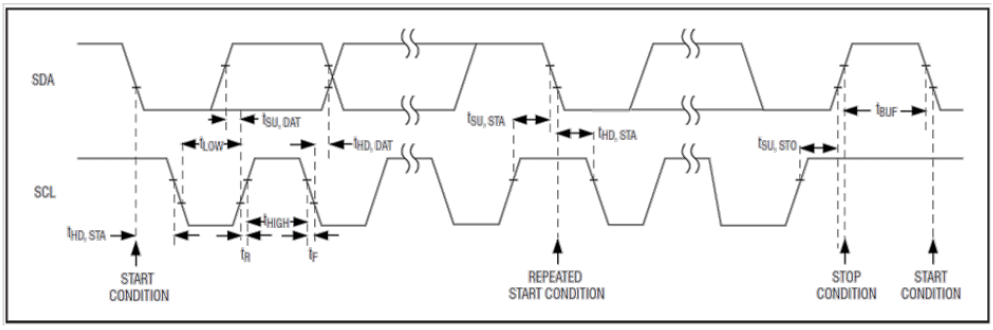

Figure 18 [20]. Schematics of the transfer protocol. Note the start condition when the SDA signal goes from high to low while SCL is high.

Instead, Figure 19 shows an example of a transmission in which a byte of data is to be written.

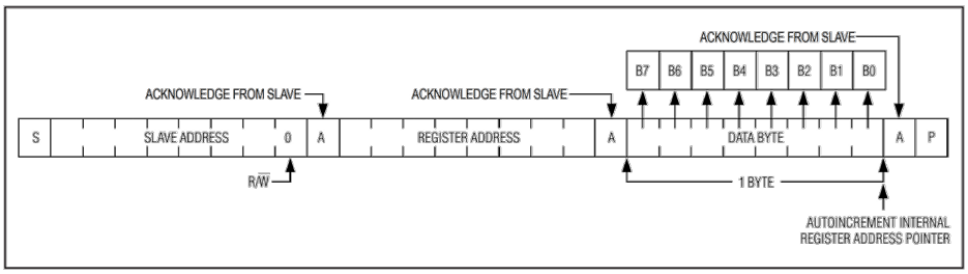

Figure 19 [20]. Schematics of a communication. It starts sending the slave address to which we want to communicate, the register address corresponding to the chosen command is then sent and finally the data byte with the settings.

Communication is then started with a start bit, followed by 7 slave address bits corresponding to the device to which the transmission is addressed. In the case of the QuadOEM these correspond to 1111000. Finally, there is a read/write bit equal to 0 if one wants to write, 1 if wants to read. An acknowledge (ACK) bit is used to make sure that the slave is ready to receive. Then it is possible to send the corresponding 8-bit register address that is used to identify the command register followed by an ACK bit. Now the data byte (thus 8 bits) is sent followed by an additional ACK and the STOP.

A good understanding of these few concepts was crucial to fully know how to program the micropumps. I then did some research on some specialized websites and I performed some simpler tests (turning on LEDs for example) to make sure I could continue to the next step.

At this point I realized that the Arduino Nano has a low baud rate, it was deemed appropriate to replace this with an STM32 Nucleo board (model L053R8) which has baud rate of 115200. The baud rate indicates the transmission speed, that is, the number of times a serial communication signal changes its states per second, in this case defined as voltage levels 0-1 (0-5 V).

Therefore, I disconnected the Arduino Nano board. It was important to keep in mind the datasheets of the Nucleo board and the Quadkey, pins D15 and D14, corresponding to SCL and SDA, were connected with the pins corresponding to A4 and A5 on the Quadkey. The 5V and Ground pins were then connected.

2.2.2. IMPLEMENTATION ON STM32CUBEIDE

I programmed the Nucleo board microcontroller to send a sequence of instructions related to the control of the micropumps. I did that in C using STM32CubeIDE software as development environment.

The programming part I carried out in the later stages was one of the most complex parts of the entire work. I started with no experience in microcontroller programming or the C programming language. I therefore carried out a training phase by asking for help from my tutor who directed me to the offices of STMicroelectronics at CNR. Then with the help of online tutorials and STM engineers, I started with the study of the microcontroller structure and the role of different pins.

Under their supervision then I resumed the operational part of the thesis development with the initialization of the pins useful to enable serial communication and communication via I2C protocol.

First, I have initialized pins PB8 and PB9 as I2C1_SCL and I2C1_SDA and pins PA2 and PA3 as USART_TX and USART_RX for serial communication (Figure 20)

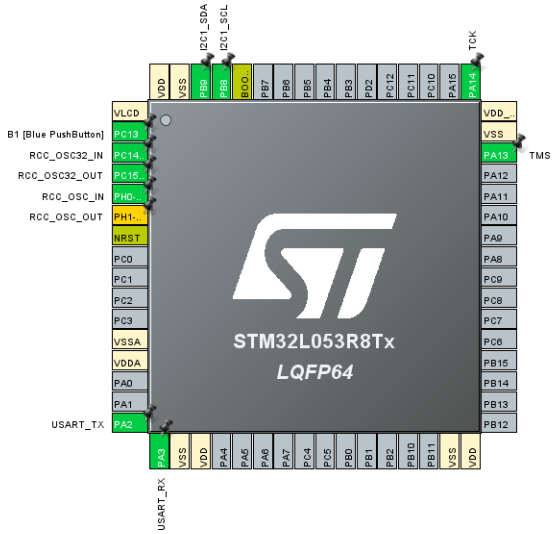

Figure 20. PIN scheme of microcontroller. PB8 and PB9 are initialized to the I2C protocol while PA2 and PA3 are initialized for serial communication

Switching then to the code, a diagram representing the sequence of commands is presented below and after that, the most important parts of the code itself.

- In the main, a unit8_t variable corresponding to the number of the micropump (n_pump) is initialized. It is used to uniquely identify each of the four micropumps.

- A memory read is performed by sending the address in hexadecimal 0x00 and read the status of the connection (this is used to verify the correct operation of the I2C protocol)

- A series of initial setup commands starts. These include:
  - An enable command to allow the QuadOEM to receive new commands.
  - A frequency setting of 200 Hz
  - A waveform configuration, in this case sinusoidal

  - Turning off all micropumps.
  - Update command

- While cycle to be executed in a loop:
  - Verification of correct operation of serial communication between the computer and the microcontroller.
  - Serial transmission that involves assigning a value to the n_pump variable
  - Switch which is based on the value of n_pump. A series of commands will be executed that have the main purpose of turning on the corresponding micropump.

```c
#include "main.h"

/* Private variables ---------------------------------------------------------*/
I2C_HandleTypeDef hi2c1;

UART_HandleTypeDef huart2;

/* USER CODE BEGIN PV */
#define MP6_ADDR 0x7B << 1 //Salve address riportato nella documentazione del Quadkey


/* USER CODE END PV */

/* Private function prototypes -----------------------------------------------*/
void SystemClock_Config(void);
static void MX_GPIO_Init(void);
static void MX_USART2_UART_Init(void);
static void MX_I2C1_Init(void);
/* USER CODE BEGIN PFP */

/* USER CODE END PFP */

/* Private user code ---------------------------------------------------------*/
/* USER CODE BEGIN 0 */

/* USER CODE END 0 */

/**
  * @brief  The application entry point.
  * @retval int
  */
int main(void)
{
  /* USER CODE BEGIN 1 */

  HAL_StatusTypeDef status;
  uint8_t n_pump;

  /* USER CODE END 1 */

  /* MCU Configuration--------------------------------------------------------*/

  /* Reset of all peripherals, Initializes the Flash interface and the Systick. */
  HAL_Init();

  /* USER CODE BEGIN Init */

  /* USER CODE END Init */

  /* Configure the system clock */
```

```
MX_GPIO_Init();
MX_USART2_UART_Init();
MX_I2C1_Init();
/* USER CODE BEGIN 2 */
uint8_t readData;
status = HAL_I2C_Mem_Read(&hi2c1, MP6_ADDR, 0x00, 1, &readData, 1, 100);

 if (status != HAL_OK)

 {
 //Transfer error in reception process

   Error_Handler();

 }



uint8_t sendData;
sendData = 0x01;
HAL_I2C_Mem_Write(&hi2c1, MP6_ADDR, 0x01, 1, &sendData, 1, 100); //00000001 Enable
sendData = 0xc0;
HAL_I2C_Mem_Write(&hi2c1, MP6_ADDR, 0x02, 1, &sendData, 1, 100); //01111111 200Hz
sendData = 0x00;
HAL_I2C_Mem_Write(&hi2c1, MP6_ADDR, 0x03, 1, &sendData, 1, 100); //11110100 Endamp on, full wave, sine
sendData = 0x00;
HAL_I2C_Mem_Write(&hi2c1, MP6_ADDR, 0x04, 1, &sendData, 1, 100); //01000000

sendData = 0x00;
status = HAL_I2C_Mem_Write(&hi2c1, MP6_ADDR, 0x06, 1, &sendData, 1, 100); //00000000 0V
if (status != HAL_OK) {
    Error_Handler();
}



sendData = 0x00;
HAL_I2C_Mem_Write(&hi2c1, MP6_ADDR, 0x07, 1, &sendData, 1, 100); //00000000 0V
sendData = 0x00;
HAL_I2C_Mem_Write(&hi2c1, MP6_ADDR, 0x08, 1, &sendData, 1, 100); //00000000 0V
sendData = 0x00;
HAL_I2C_Mem_Write(&hi2c1, MP6_ADDR, 0x09, 1, &sendData, 1, 100); //00000000 0V
sendData = 0x01;
HAL_I2C_Mem_Write(&hi2c1, MP6_ADDR, 0x0A, 1, &sendData, 1, 100); //Update

/* USER CODE END 2 */

/* Infinite loop */
/* USER CODE BEGIN WHILE */
```

```
while (1)
{

    if(HAL_UART_Receive(&huart2, &n_pump, 1, 100)==HAL_OK){

    HAL_UART_Transmit(&huart2, &n_pump, 1, 100);

       switch(n_pump){

        case '1':
            //HAL_UART_Transmit(&huart2, &n_pump, 1, 100);
            sendData = 0x1f;
            HAL_I2C_Mem_Write(&hi2c1, MP6_ADDR, 0x06, 1, &sendData, 1, 100); //00011111 250V peak
            sendData = 0x00;
            HAL_I2C_Mem_Write(&hi2c1, MP6_ADDR, 0x07, 1, &sendData, 1, 100); //00000000 0V
            sendData = 0x00;
            HAL_I2C_Mem_Write(&hi2c1, MP6_ADDR, 0x08, 1, &sendData, 1, 100); //00000000 0V
            sendData = 0x00;
            HAL_I2C_Mem_Write(&hi2c1, MP6_ADDR, 0x09, 1, &sendData, 1, 100); //00000000 0V
            sendData = 0x01;
            HAL_I2C_Mem_Write(&hi2c1, MP6_ADDR, 0x0A, 1, &sendData, 1, 100); //Update
            break;

        case '2':
            //HAL_UART_Transmit(&huart2, &n_pump, 1, 100);
            sendData = 0x1f;
            HAL_I2C_Mem_Write(&hi2c1, MP6_ADDR, 0x07, 1, &sendData, 1, 100); //00011111 250V peak
            sendData = 0x00;
            HAL_I2C_Mem_Write(&hi2c1, MP6_ADDR, 0x06, 1, &sendData, 1, 100); //00000000 0V
            sendData = 0x00;
            HAL_I2C_Mem_Write(&hi2c1, MP6_ADDR, 0x08, 1, &sendData, 1, 100); //00000000 0V
            sendData = 0x00;
            HAL_I2C_Mem_Write(&hi2c1, MP6_ADDR, 0x09, 1, &sendData, 1, 100); //00000000 0V
            sendData = 0x01;
            HAL_I2C_Mem_Write(&hi2c1, MP6_ADDR, 0x0A, 1, &sendData, 1, 100); //Update
            break;

        case '3':
            //HAL_UART_Transmit(&huart2, &n_pump, 1, 100);
            sendData = 0x1f;
            HAL_I2C_Mem_Write(&hi2c1, MP6_ADDR, 0x08, 1, &sendData, 1, 100); //00011111 250V peak
            sendData = 0x00;
            HAL_I2C_Mem_Write(&hi2c1, MP6_ADDR, 0x06, 1, &sendData, 1, 100); //00000000 0V Pompa
            sendData = 0x00;
            HAL_I2C_Mem_Write(&hi2c1, MP6_ADDR, 0x07, 1, &sendData, 1, 100); //00000000 0V Pompa
            sendData = 0x00;
            HAL_I2C_Mem_Write(&hi2c1, MP6_ADDR, 0x09, 1, &sendData, 1, 100); //00000000 0V Pompa
            sendData = 0x01;
            HAL_I2C_Mem_Write(&hi2c1, MP6_ADDR, 0x0A, 1, &sendData, 1, 100); //Update
            break;
```

```
          case '4':
              //HAL_UART_Transmit(&huart2, &n_pump, 1, 100);
              sendData = 0x1f;
              HAL_I2C_Mem_Write(&hi2c1, MP6_ADDR, 0x09, 1, &sendData, 1, 100); //00011111 250V peak
              sendData = 0x00;
              HAL_I2C_Mem_Write(&hi2c1, MP6_ADDR, 0x06, 1, &sendData, 1, 100); //00000000 0V
              sendData = 0x00;
              HAL_I2C_Mem_Write(&hi2c1, MP6_ADDR, 0x07, 1, &sendData, 1, 100); //00000000 0V
              sendData = 0x00;
              HAL_I2C_Mem_Write(&hi2c1, MP6_ADDR, 0x08, 1, &sendData, 1, 100); //00000000 0V
              sendData = 0x01;
              HAL_I2C_Mem_Write(&hi2c1, MP6_ADDR, 0x0A, 1, &sendData, 1, 100); //Update
              break;

          default:
              //HAL_UART_Transmit(&huart2, &n_pump, 1, 100);
              sendData = 0x00;
              HAL_I2C_Mem_Write(&hi2c1, MP6_ADDR, 0x09, 1, &sendData, 1, 100); //00011111 250V peak
              sendData = 0x00;
              HAL_I2C_Mem_Write(&hi2c1, MP6_ADDR, 0x06, 1, &sendData, 1, 100); //00000000 0V
              sendData = 0x00;
              HAL_I2C_Mem_Write(&hi2c1, MP6_ADDR, 0x07, 1, &sendData, 1, 100); //00000000 0V
              sendData = 0x00;
              HAL_I2C_Mem_Write(&hi2c1, MP6_ADDR, 0x08, 1, &sendData, 1, 100); //00000000 0V
              sendData = 0x01;
              HAL_I2C_Mem_Write(&hi2c1, MP6_ADDR, 0x0A, 1, &sendData, 1, 100); //Update
              break;

            }
      }


  }
    /* USER CODE END WHILE */

    /* USER CODE BEGIN 3 */

  /* USER CODE END 3 */
}

/**
  * @brief System Clock Configuration
  * @retval None
  */
void SystemClock_Config(void)
{
  RCC_OscInitTypeDef RCC_OscInitStruct = {0};
  RCC_ClkInitTypeDef RCC_ClkInitStruct = {0};
```

Figure 21 Code uploaded in the microcontroller

A major problem also arose during the code writing phase. Once the code was loaded onto the microcontroller, the commands to turn the power on and off and to set various parameters seemed not to work. I realized that the problem was not conceptual and in how the code was implemented but in the “unusual” need for the QuadKey to receive an update command to update its parameters and thus to turn on micropumps (to be noticed the Update command at the end of each write-to-memory sequences)

Serial communication allows micropump control command to be sent either from the keyboard or from external programs as long as they allow the opening and closing of serial communication.

The following example explains the programming strategy I adopted.

Suppose one wants to turn on micropump 1. From the register table (not shown for reasons of available space) it can be seen that the register address corresponding to Power Mode is 0x01. Checking now on the manual [20] the data bits to be sent, these must be 7 random bits and one bit 0 or 1, with 1 corresponding to Enable. Therefore the code should be:

```
HAL_I2C_Mem_Write(&hi2c1, MP6_ADDR, 0x01, 1, 0x01, 1, 100);
```

The function used is Mem_Write because the intention is to write to memory, this takes as input the type of protocol used (hi2c1), the slave address MP6_ADDR defined for convenience on an early stage of the code, the register address in hexadecimal, its size (1 byte), the data bits to be written in hexadecimal 00000001 (0x01), its size, and the timeout. This is followed by a series of similarly formulated commands, in this case the power on/off command is controlled, which for the purposes of this thesis is of main relevance. From the register table it can be read that the address corresponding to the voltage regulation of micropump 1 is 0x06. Therefore, having to turn it on, we can read that the structure of the byte to be sent provides three bits for the output ramp time setting while the remaining five bits concern the peak voltage of each output with 00000 corresponding to 0 V (micropump off) and 11111 corresponding to 250 V (micropump on). Therefore, the command to be sent has the following structure.

```
HAL_I2C_Mem_Write(&hi2c1, MP6_ADDR, 0x06, 1, 0x1f, 1, 100);
```

Attention is drawn to 0x1f corresponding to 11111111 in hexadecimal.

It is specified that this command is located within the switch in "case 1" and will be activated when the value 1 is read via serial.

2.2.3. MICROPUMPS CONTROL INTERFACE ON LABVIEW

This first approach to implementation in LabVIEW was fairly straightforward. With the help of tutorials on the websites, I was able to understand how LabVIEW's VISA library works, and with some elementary basics, I was able to plug in the part of programming done up to this point.

Starting without some basics of even this programming language, I did, at an early stage, short exercises outside of the topics of this thesis to become more familiar with object-oriented programming languages. Then I resumed the workflow of my thesis.

I carried out the implementation in LabVIEW with the use of the serial palette and specifically using the library of VISA functions that allow serial communication to take place.

Within an event structure there is the following series of steps:

- Opening serial communication by opening port COM5 with baud rate 115200 and turning on virtual led.
- Wait 100ms to avoid any latency problems (LabVIEW software level).
- Case structure separating cases:
    - Manual control of micropumps via virtual button on front panel.
    - Automatic control of micropumps defined by a sequence of commands set in a previous step.
- Within the case structure the sending of bits via serial takes place, so by means of a command provided with either of the above methods a serial will be sent to the microcontroller, which will send the corresponding sequence of commands defined by the switch whose operation was previously explained.
- While cycle necessary for the second event of the case structure defined above, the operation of which in detail will be explained later. It waits until the process ends.
- Closing serial port and turning off the virtual led.

During this phase some issues raised. The major one was to take trace of the opening/closing process of the serial port. The channel can be opened only by one application per time so it’s important to remember to close it after each operation. It happened frequently that I tried to open the serial port from LabVIEW during my tests but the serial port was already opened in the Cube IDE of STM (the IDE I used for programming the microcontroller). I had also to keep attention to

the baud rate, it was important to follow the technical specifications of the Nucleo microcontroller manual.

I encountered also a sort of "bug" in the interaction between the synergic execution of the code in the microcontroller and the code in LabVIEW. The execution in LabVIEW tends to be too much fast and it seems that the opening of the serial port and sending the message was not so fast. The result was that the port COM5 did not have enough time to open properly before the serial message was sent, so the result was that the message did not arrive to the microcontroller, thus not giving the possibility to control the micropumps properly. So, it was crucial to put just a 100ms timer between the command to open the serial port and the command to send a message via serial port (the timer is in the second section of the block diagram).

In Figure 22 is presented the block diagram

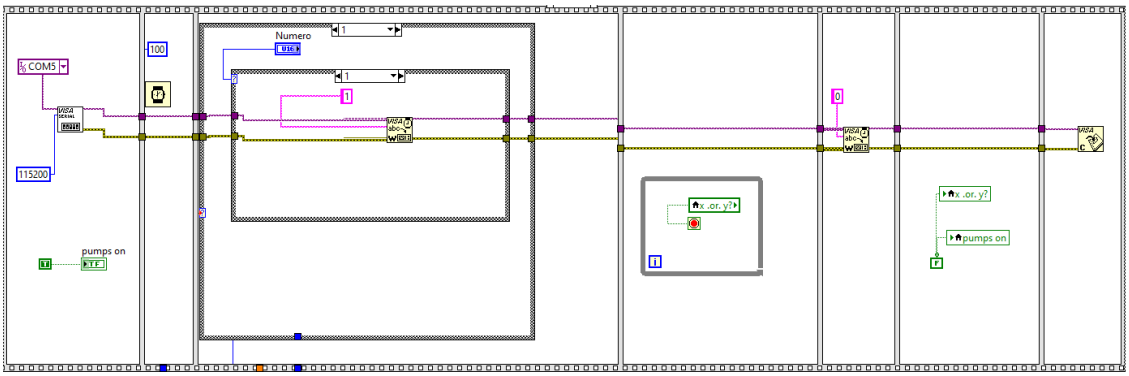

Figure 22. Block scheme for micropumps control. From left to right: opening of COM5 and setting baud rate to 115200, wait 100 ms, serial communication (micropump to turn on), wait cycle to "wait" until the process ends, turn off the micropump, set flags to False, close serial communication

As mentioned in the case structure, I programmed the micropumps to operate in two different ways. The first is to manually turn on/off using the appropriate numbered buttons corresponding to the number of micropumps to be turned on/off. In this case, a value corresponding to the micropump to be controlled is simply provided. This can be a useful function to have more control on flows and in stages such as the initial one where one would like to fill the tubes with liquid before proceeding with the sequence of procedures.

The second operation involves automatically turning on the micropumps by command that was provided at an earlier stage. The command corresponding to the micropumps involves providing the number of pumps to be turned on and the amount in *mL* of liquid to flow. In this case, a timing

system will be activated in which using information about the flow rate of the micropumps, it will be possible to calculate in milliseconds how long the micropump is to be turned on and to adjust its shutdown. The while loop discussed earlier delays the execution of the micropump shutdown command until the end of the timer. A progress bar on the front panel allows the execution progress of the command to be displayed. A STOP button allows the operation of the micropumps to be stopped in a preventive manner.

Below is a picture of the control system on the front panel.

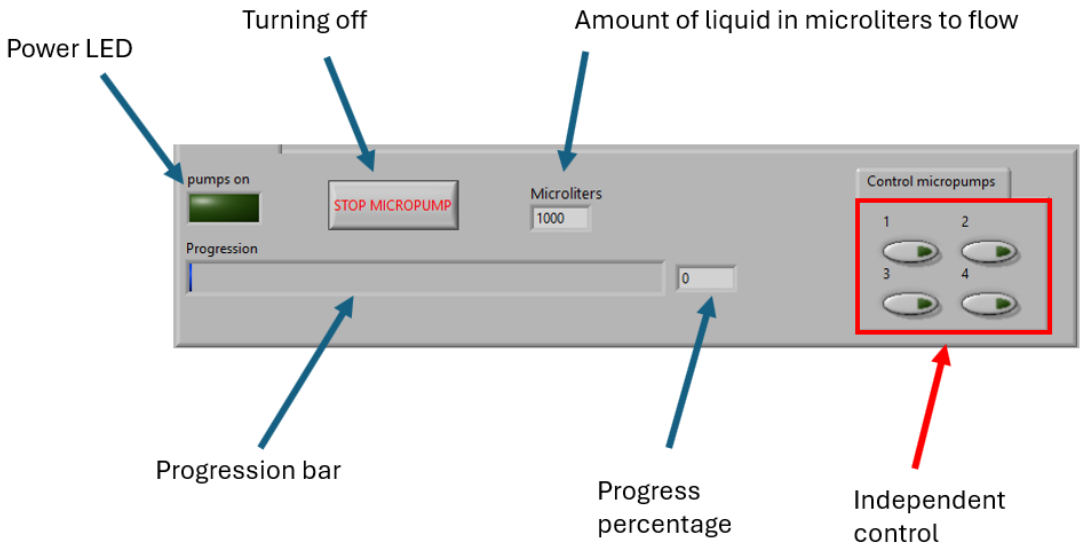

Figure 23. Virtual front panel on LabVIEW for the control of micropumps

2.3 AUTOLAB CONTROL

As previously mentioned, the application provides a system to control the Autolab in order to perform the measurements. Before the implementation could be carried out in LabVIEW, it was necessary for me to have a clearer understanding of the functioning of the Autolab and the software used to make the measurements. The model used is Autolab PGSTAT204 (Figure 24), includes a potentiostat/galvanostat with uniform voltage of 20 V and maximum current of 400 mA [21].

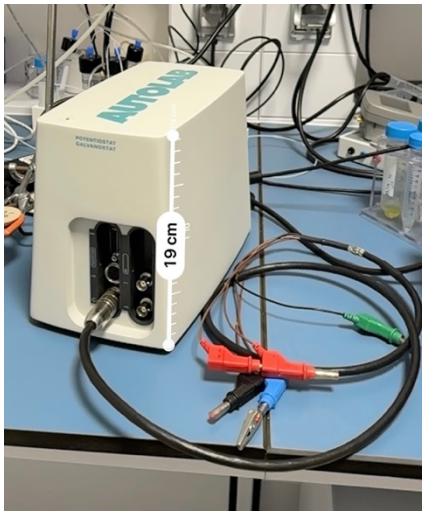

Figure 24. Photo of the Autolab PGSTAT204

As can be seen from the figure above a cable is connected to the instrument that splits into additional smaller cables that terminate with ferrules so that they can be connected either to alligator clips or to a dummy cell. I have carried out preliminary tests on a dummy cell and following the manual instructions to better understand how the instruments works.

Control of the instrument is done from the computer using Nova software [22]; version 2.1 was used for this thesis work. The software interfaces with the Autolab using procedures that the operator can load or create on the fly. These procedures are presented as a sequence of operations that are executed as they are performed. In Figure 25 there is an example of a procedure for performing a DPV.

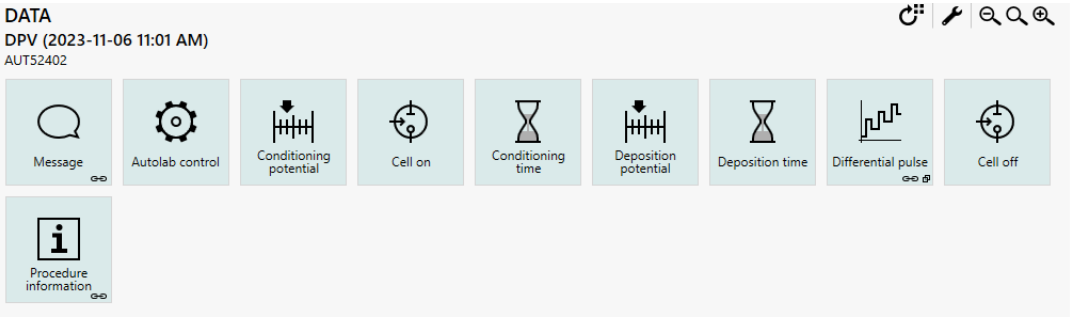

Figure 25. Procedure example. From left to right: Message of start, Autolab control settings, set conditioning potential, turning on the cell, conditioning time (wait), set deposition potential, deposition time (wait), set differential pulse parameters, turning off the cell, overall information of the procedure

Each procedure is presented with a block diagram, each block has within it a series of parameters and respective values that the software sends to the Autolab the moment the measurement is started. Of particular interest for the purpose of this thesis is the "Differential Pulse" block, within it, as can be seen from Figure 26, a number of parameters are adjustable, like parameters that adjust the type of ramp.

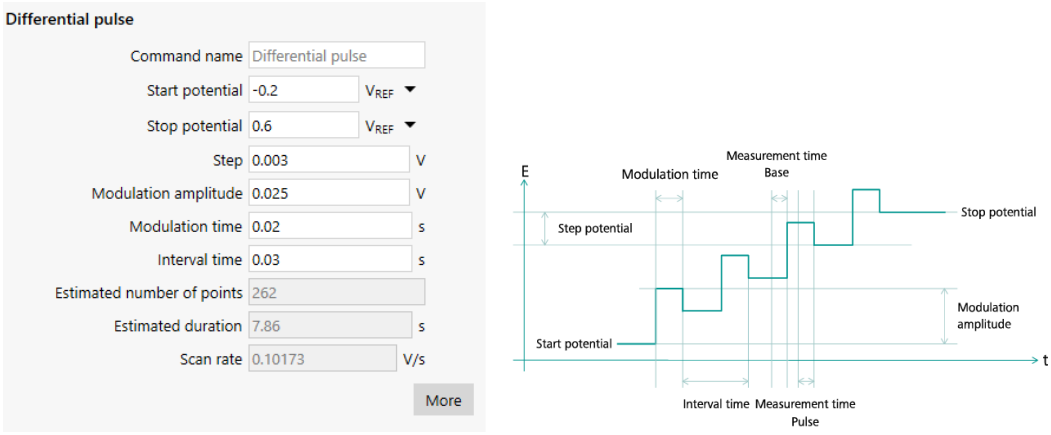

Figure 26. Left: Example of parameters used in a Differential Pulse Voltammetry measures as can be seen from the Nova software. Right: Physical meaning of each parameter [22]

Each procedure is then saved as a .nox file. Once this is done, it is possible to proceed with implementation in LabVIEW.

2.3.1 LABVIEW IMPLEMENTATION AND INTERFACE DESCRIPTION

The Autolab SDK manual [23] provides guidance on implementing an Autolab control system. Specifically, once I have downloaded all packages, a folder will be created with some starting sub_VIs.

The next phase was crucial. With the help of the manual and a few sub_VIs downloaded in the basic package with the Autolab SDK for LabVIEW, it was necessary to build the main body of the VI through which the various devices were to be connected and run synergistically. Once again before starting to program block diagram, it was first necessary to make a thorough study of the available material and in particular the available sub_VIs. This kind of work, in addition to being particularly complex, took several weeks, and once again I asked for help in advanced programming in LabVIEW and in reading block diagrams. These in fact were particularly complex, and no description or commentary was provided in the manual to help in understanding in detail the individual components of the diagram. The complexity of the work to be done and the amount of detail that had to be taken into account also led me to make a preliminary plan for the structure of the main_VI.

Also the same sub_VIs provided by Metrohm were not totally implemented correctly. I had to implement some of them again from an interpretation of the initial plan of the VI. In order to get some clarifications, I also contacted the people responsible for the software version of the instrument but they could not give me any explanations.

This main_VI is the final product obtained as a result of these events.

The structure is described below.

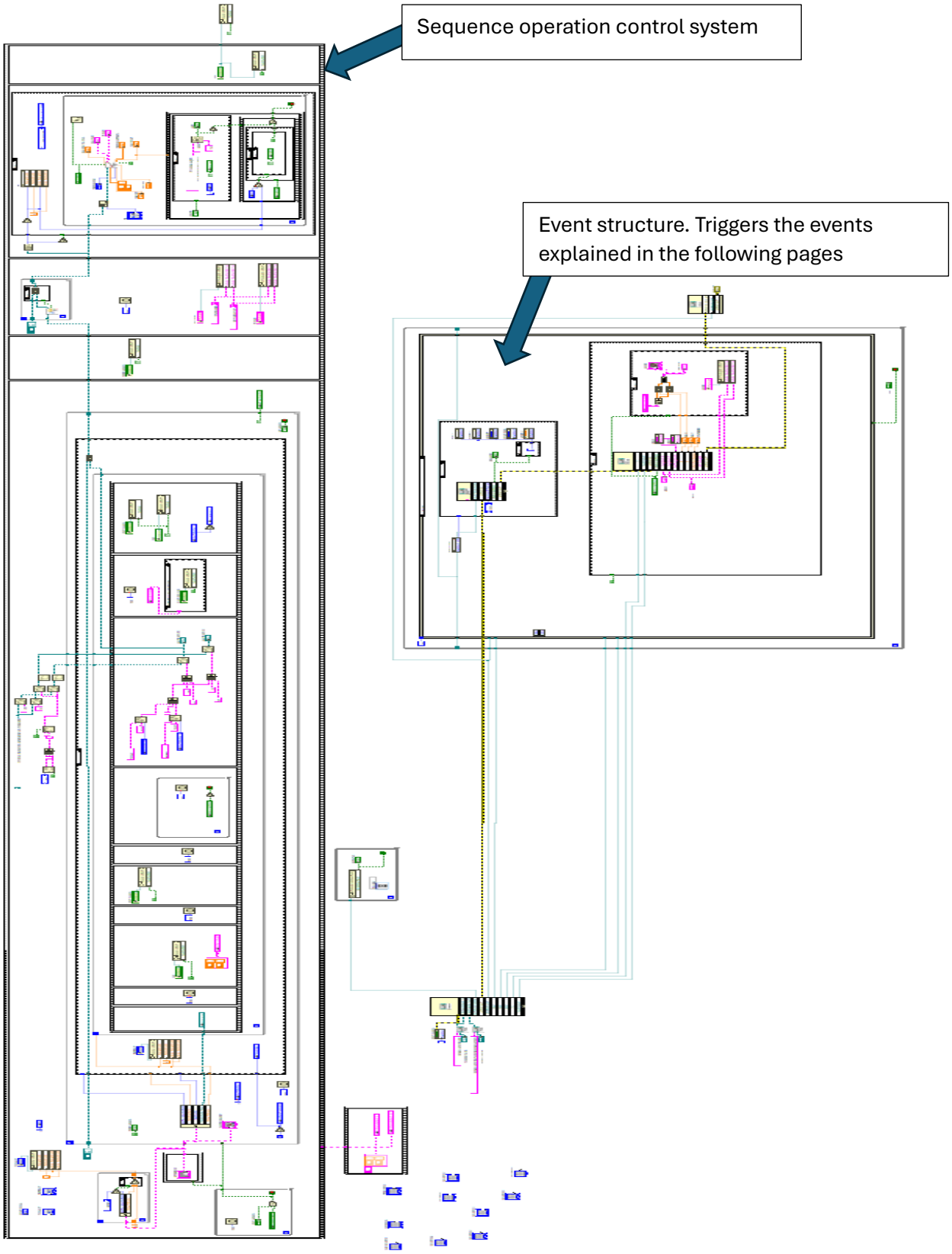

Figure 27. Block diagram of the main VI

I had the idea to divide the main_VI into two main macro-components: an event system for command execution and an event sequence control system. In computer science terms, one could call the event system as “low-level”, and the sequence control system as “high-level”.

The event system, in fact, controls the basic commands and settings, thus how a measurement is performed, with which parameters, the connection system and any settings. This section thus includes all those sub_VIs that perform as basic functions.

The sequence system, on the other hand, controls these events "from above." Starting from the sequence of operations entered by the operator, an element is extracted from time to time, and the corresponding events entered in the previous system will be called.

My idea to proceed in this way came after realizing that the final product would be particularly complex, especially as the number of components and factors to be taken into account. In fact, the structure I realized, ensures that I could have more order within the diagram and have the ability to take precise action at a particular point in the diagram in case some change was to be made or some errors were present. Therefore, such a structure provides me with the ability to take precise action at specific points in the diagram without the need to make excessive general changes in the entire VI.

2.3.1.1 Connection control

It consists mainly of a sub_VI that takes in the Autolab system files (adk.x and HardwareSetup.exe). It gives back a signal that in case of a successful connection turns on the "isConnected" led. Turning on the led is embedded in a while loop that repeatedly checks the connection status. Several parameters useful in the measurement phase also exit from the sub.

2.3.1.2 Event structure

Once the connection is made, a while loop governed by a 100ms timer occurs, from which it is possible to exit with a STOP button. Within this there is an event structure. Each event is called as a result of a condition being met. This condition can be a type of button pressed, a type of procedure loaded, or a type of operation to be performed.

2.3.1.3 Timeout

The "default" mode. The system waits for the "start measure" procedure to be activated so that the type of procedure loaded can be taken and then parameters are read. When the procedure is triggered, the Sampler will begin to collect data which, based on the values provided by Signal X and Signal Y of the graph, it will be displayed on the "Sampler graph". It should be specified that

the data collected in this way is not for all intents and purposes of the measurement data but should be reputed as real time "acquisition" of the voltage, current and time values of the instrument.

The actual measurement data is obtained by loading and setting the correct representation of the parameters unique to each type of procedure, but this will be seen later. If the user wants, for example, to perform a DPV measurement, a correct representation and display of this involves representing on a graph the differential current (delta current), given by the difference between pulsatile current and base current, with respect to the applied potential. The delta current is thus a parameter that is "derived" from other parameters; therefore, it can only be displayed by loading the appropriate DPV procedure. In addition, in the case of cyclic voltammetry or again differential pulse voltammetry measurements, the voltage values obtained from the sampler also contain all those voltage values over which the instrument passes before reaching the starting voltage. Thus if a ramp from -0.2 V to 0.6 V is expected on the sampler all those voltage values that the instrument passes over to go from 0 V to -0.2 V at the start of the measurement and all those values to go from 0.6 V to 0 V at the end of the measurement will be collected. Also I had to keep in mind that the sampler has a sampling period of 100ms (the duration of each while cycle), but the sampling of each measurement is usually faster. It is therefore appropriate to consider the sampler for the purpose of "real-time display" of measured voltage/current values but not for measurement purposes.

2.3.1.4 Load

Another event of relevance is “Load”. Here I load the procedure related to the measurement to be made. A sub_VI called "load" takes in the procedure and returns a string parameter that will enter the sub_VI "param" that will return an array in which the type of procedure is defined (e.g., DPV or CV measurement) and all the parameters associated with it. In particular, a Case structure was then constructed that, based on the first value in the array, i.e., the name of the procedure (always CV or DPV), will go on to extract procedure parameters (e.g., parameters to define a ramp for a CV). These parameters will then be displayable on the front panel as shown in Figure 28.

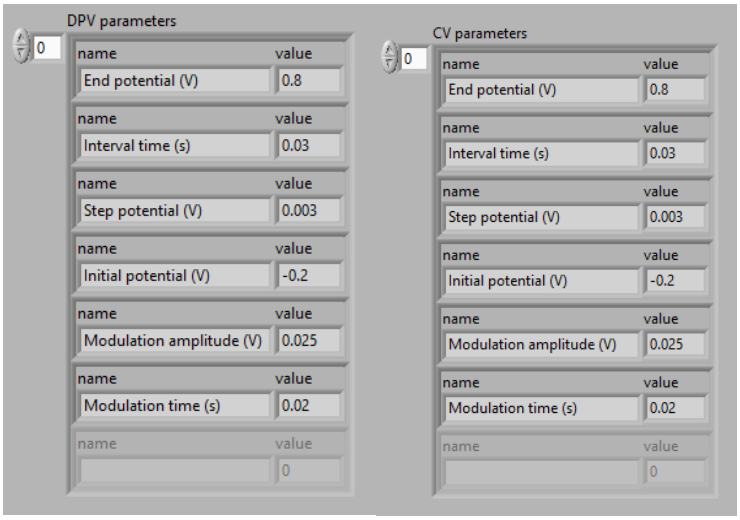

Figure 28. Examples of parameters and their values that can be seen from the front panel of the Autolab control in LabVIEW.

The name of the procedure will define the activation of the next two events.

2.3.1.5 Start measure and abort measure

The “Start measure” is the measurement startup procedure, turning on the "isMeasuring" LED and calling the following pair of events.

The event “abort measure” is triggered instead by pressing the corresponding button and is used to interrupt the current measurement.

2.3.1.6 DPV data / CV data

The invocation of these events is handled automatically by the application and is controlled by the first array value that is read in param (thus the name of the procedure).

Both Sub_VIs work similarly although the parameters they recall are different. Thus, if the first parameter read is CV the CV data event will be triggered. The measurement parameters Time, Potential and Current will then be called, which once the measurement is taken will be filled in as an array with the respective measured values. In a similar manner DPV data works but the parameters called are Time, Potential Applied, Pulse Current and Base Current. From the latter two, the fifth parameter Delta Current will then be derived. Potential and Current in the case of cyclovoltammetry measurement and Potential Applied and Delta Current in the case of differentiated voltammetry will then be displayed on the graph. The data so collected will be organized into matrices and will be used for the saving step that will be explained later.

2.3.1.7 Sequence control structure

Once the basic structure of the application has been established, the main control system, i.e., control of the sequence of operations, can be defined.

The main steps will be described below.

- Definition of an array called Operation List, here all operations with related parameters are included. In particular, an operation with Autolab (thus electrochemical measurement) will be associated with the related procedure; an operation with micropumps will be associated with an integer corresponding to the number of micropumps to be turned on and the amount of solution to be moved.
- Initialization all parameters to bring them to a "steady state"
- Check connection with the instrument in logic END with the START SEQUENCE button on the front panel. This is the exit condition from a while cycle that will occur only when isConnected and START SEQUENCE are both at 1. The cycle exit determines the start of the sequence of operations to be performed.
- For loop in which one operation will be processed at a time: within it, each operation is divided by its parameters.
- Case structure controlled by the first parameter of the current operation, the name of the operation (Autolab or micropumps)
    - Operation micropumps: sequential structure in which using the reference to the trigger button of the "micropumps" event (illustrated above) activates the event by sending as input the parameters previously entered by the operator.
    - Autolab operation: sequential structure in which using the reference to the trigger button of the "Start measure" event (illustrated above) activates the event by sending as input the parameters previously entered by the operator. Once the measurement is executed, the method for saving the measurement is performed. This will be illustrated later.
- Exit the sequence and move to the post-processing phase.

Figure 29 is a screenshot of the front panel and specifically the panel to control the operations to be executed.

Once a list of operations has been defined, the operator can start the sequence by pressing the START SEQUENCE button, the "Running sequence" LED will then light up and in "executing"

he will be able to see the operation being executed. "Current operation" defines the operation number of the running sequence. It should also be noted that by varying the value of "Repeats" it will be possible to execute the same operation several times with the same parameters. There is an EXIT SEQUENCE button to exit the sequence in the event in the case for example some operations were entered incorrectly, and a Stop Main button that will stop the entire application.

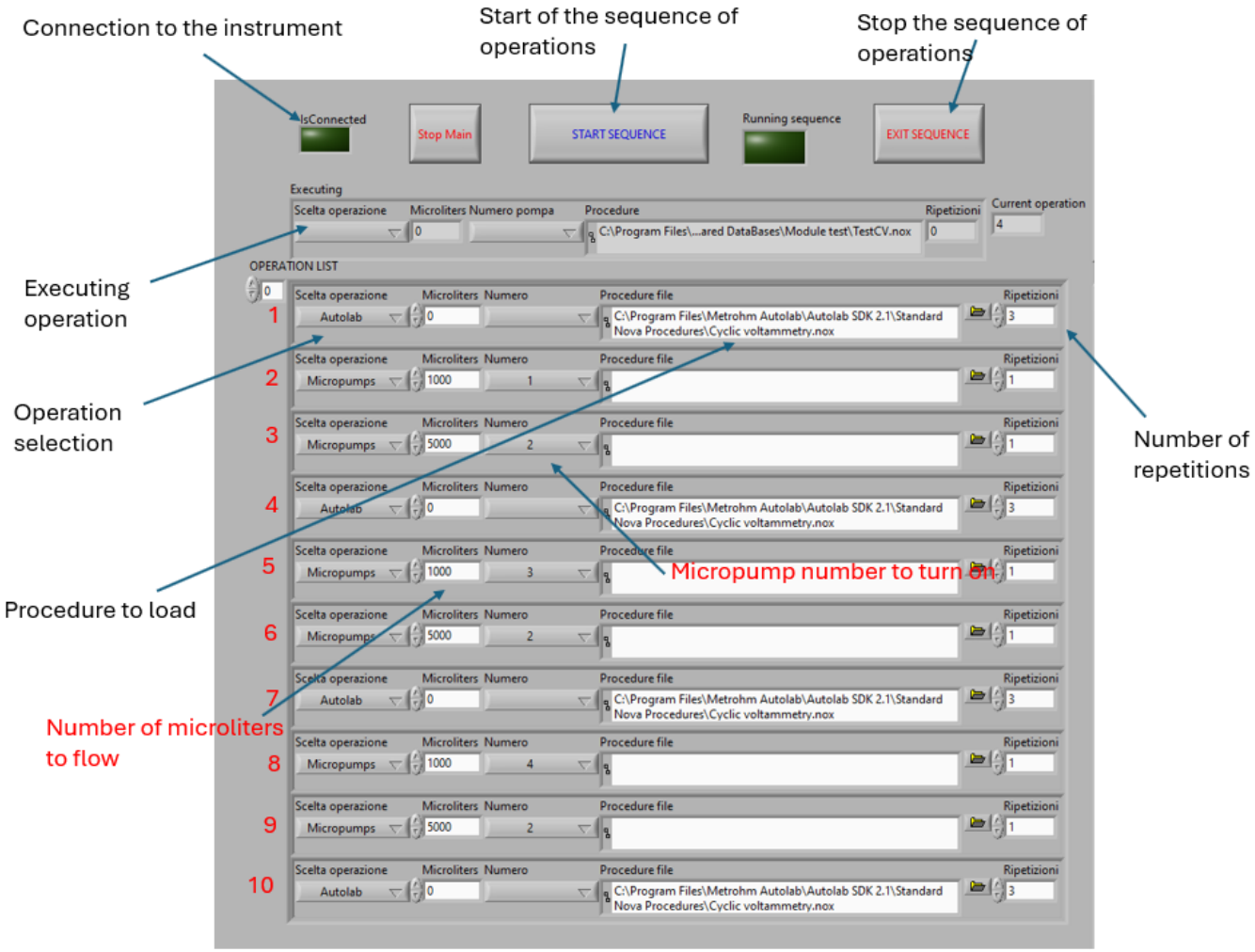

Figure 29. Front panel, operation selection section

Instead, Figure 30 is a screenshot of the front panel dedicated to displaying measurements.

In the panel is present an "isMeasuring" LED that lights up the moment a measurement starts. There is an "Abort" button to stop the measurement. There is also the possibility to select the parameters to be displayed on the X-axis and Y-axis of the Data Sampler. The values of these parameters can also be displayed along with the applied potential.

The graph section is divided into four parts:

- Data Sampler for displaying the data collected by the Sampler in Timeout (operation illustrated above).
- Last Measure for displaying the last measurement acquired (not in real time).
- All DPVs for the display of all curves obtained by DPV data in the current sequence of operations.
- All CVs for the display of all curves obtained by CV data in the current sequence of operations.

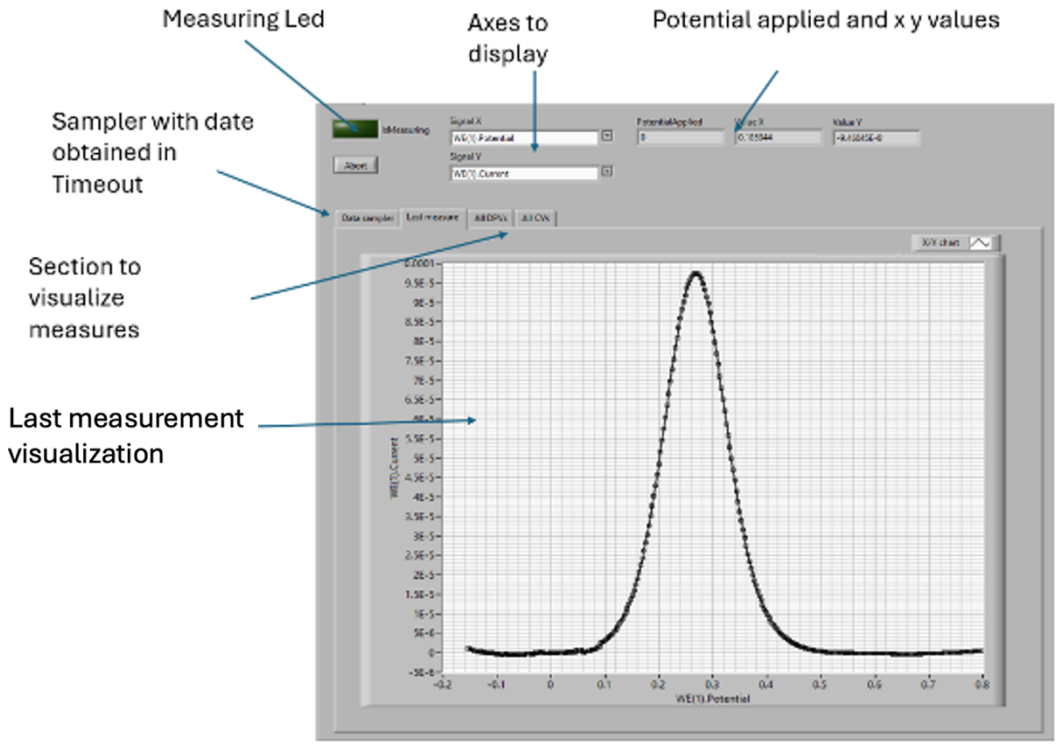

Figure 30. Front panel, Autolab measure section

2.3.1.8 Saving measures

The saving system is also automatic after the end of each measurement. Once the application is started, it will check that a folder named "Measurements" within the project directory exists, otherwise it will be created; two subfolders named "DPV" and "CV" will then be also created if they do not already exist.

When the START SEQUENCE button is pressed, the application will create in both subfolders another folder named with the date and time at which the sequence started. The application will automatically sort the files obtained from CV measurements and those obtained from DPV measurements. Each file will automatically be named with the operation number and the repetition number so that each measurement can be uniquely defined.

To conclude for both CV and DPV measurements, the file that is saved presents a header in which the measurement parameters are saved, which are those shown in Figure 28. Thus, for CVs three columns corresponding to Time, Potential, Current are saved while for DPVs five columns corresponding to Time, Potential, Base Current, Pulse Current and Delta Current are saved.

2.4 DATA PROCESSING AND BASELINE CALCULATION METHODS

The next part is a bit “trickier”. It required a preliminary study of some literature articles as well as some knowledge in mathematics. It can be considered more of software level phase because there are no hardware elements to integrate. However, it turns out to be interesting because proper implementation of this part greatly simplifies the post-processing phase that comes after acquiring each electrochemical measurement.

The post-processing phase essentially consists of applying various methods to obtain the baseline for a DPV curve. As explained in the first chapter, the calculation of the baseline turns out to be crucial because it allows the derivation of measurement data such as area and peak height. The importance of the accuracy with which the calculation is done is also noted. An incorrectly defined baseline leads to measurement data that may not even be meaningful at all. In the present work, the methods for performing this calculation have been divided into three types: manual, semi-automatic and automatic methods. In the literature there is a large number of algorithms used for detection/correction as automated as possible of the baseline, in this thesis some of them will be mentioned and additional ones presented. It is also necessary to highlight that even the most automated of methods must always be accompanied by a "visual" verification since, the high variety of possible shapes of DPV curves that could be obtained clashes with a not so high flexibility of the algorithm. Thus the possibility of making mistakes persists.

Following paragraphs show different methods and algorithms progressively more complex that I studied for the baseline calculation. I made also different kind of tests with different curves (shown in the next pages) and compared different methods with the aim to understand if I can derive a "rule" to build my automatic algorithm. The aim is always to try to reduce the number of parameters required from the algorithm and if there is a way to choose the value of the few of them I have chosen to use.

2.4.1 MANUAL METHOD

The main method among those belonging to this category is to select a range of points on the DPV curve to perform a polynomial fit. The following is an example.

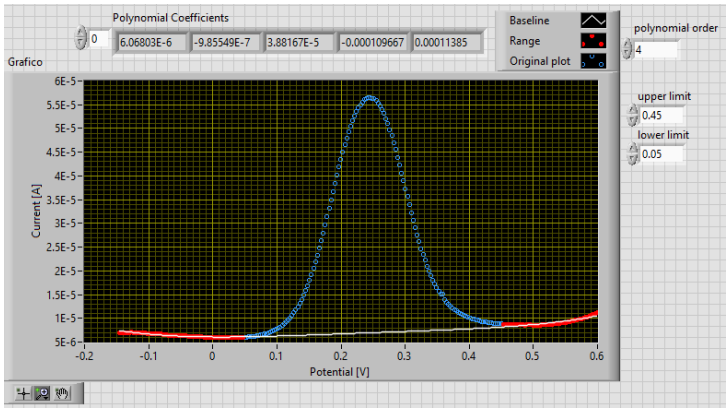

Figure 31. Polynomial fit with point selection. In red the selected points to be used for the fit of the curve. In blue the original curve while in white the baseline calculated.

In Figure 31 it can be seen in blue the original DPV curve on which we want to calculate a baseline. We start by defining an upper and lower limit. For the fit of the polynomial all those points below the lower limit and above the upper limit will be taken. In this case lower limit has been set to 0.05 V while the upper limit to 0.45 V, on the graph they are highlighted in red.

The degree of the polynomial is now chosen. There is no one-size-fits-all criterion for the choice, generally it can be used a degree 3 or 4 for simpler, i.e., more "flat" curves at the extremities and a degree 6, 7 or 8 polynomial for more complex curves, such as the one presented in Figure 32.

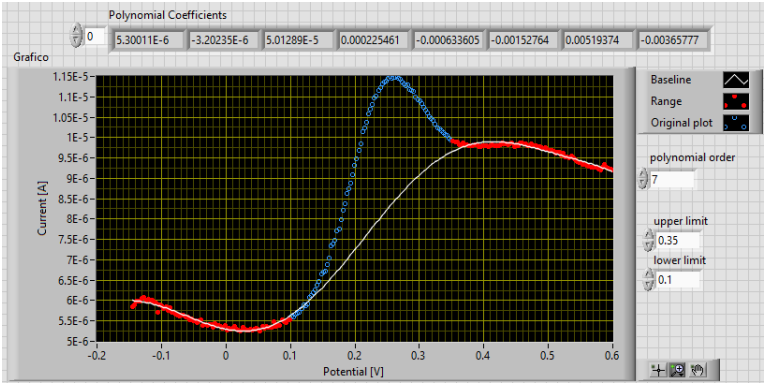

Figure 32. Polynomial fit with 7th degree polynomial, more complex than the one presented in Figure 31 so it's required an higher polynomial degree to calculate the baseline

In this case the flat DPV curve is less visually intuitive and the acceptable plotting of the baseline requires the use of a polynomial of degree 7 therefore with a more complex shape.

In both cases it can be seen the baseline (in the figure shown in white) and the corresponding coefficients of the polynomial.

Once such operation has been performed it is possible to proceed with the subtraction of the baseline from the original curve. The result is a "flattening" of the DPV curve allowing only the shape of the peak to stand out.

Figure 33 and Figure 34 are the results of the subtraction operation.

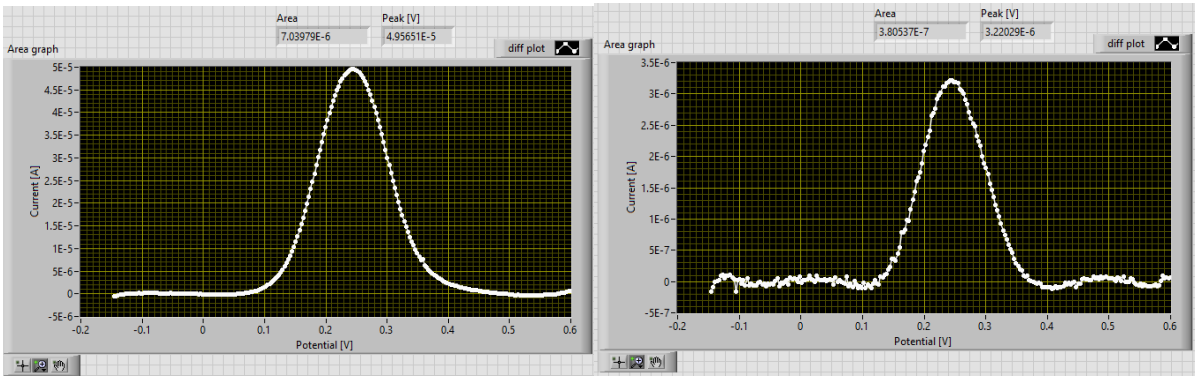

Figure 33. subtraction of the baseline made on the first curve with grade 4 polynomial. Figure 34. Subtraction of the baseline made on the first curve with grade 7 polynomial

From the curves obtained in this way it is then possible to derive the peak height and the area under the curve. Both are calculated and are shown at the top of the graphs.

Note also the more "unstable" profile of the second curve due to an imperfect overlap of the baseline with the original curve. This type of issue can be at least partially overcome if instead of adopting a range of points of the type:

[start – lower limit] U [upper limit - end]

A range pair of this type is chosen:

[lower limit 1 – upper limit 1] U [lower limit 2 – upper limit 2]

Thus, this method involves selecting a double range of points. We see below a possible result.

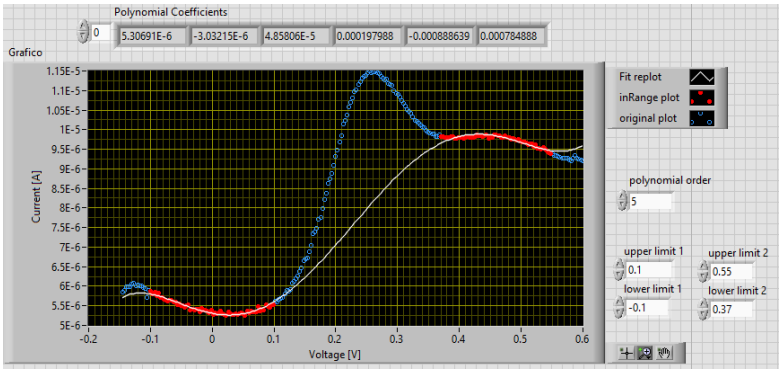

Figure 35. Polynomial fit executed with four limits

In this case it can be seen that two ranges (in red) have been defined to obtain the baseline curve. This allows the use of a polynomial of lower degree thus allowing the baseline trend to be "relaxed" at the ends. The ends, in fact, may have a complex trend to follow, in addition to the fact that a larger selection of points to fit may involve the use of a higher degree polynomial. Such a method allows the curve fit to be more focused on a selection of points of greater interest. Also keep in mind that all points being fit have exactly the same weight, regardless of whether they are closest to or furthest from the peak area.

The result of the subtraction is as follows.

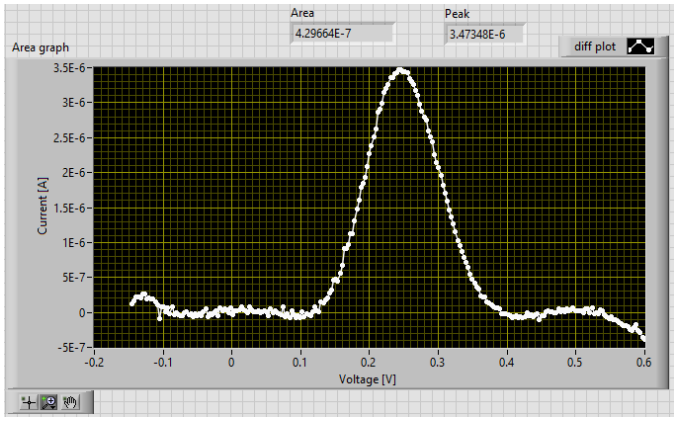

Figure 36. Result obtained with the fit using four limits and a 5th grade polynomial. Note how the result is similar to the one obtained with the 7th grade polynomial but using a lower number of points.

It can be seen that the results of area and peak are comparable between the two methods although the results obtained by the second method are slightly higher.

It would also be possible to "extreme" this method by selecting a smaller number of points and use a polynomial of even lower degree as in the case below.

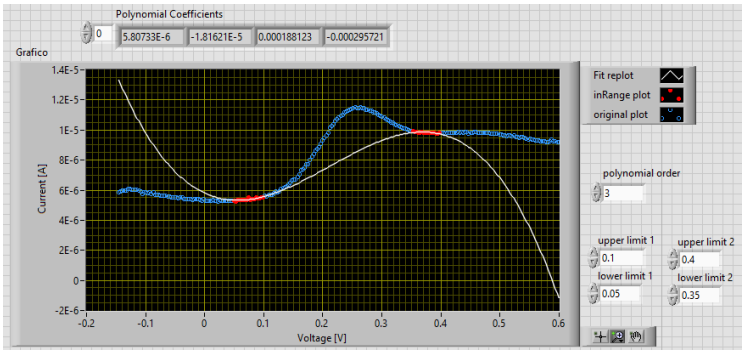

Figure 37. Fit with a smaller number of points used and with a lower polynomial degree.

When evaluating areas, therefore, everything below the lower limit 1 and above the upper limit 2 can be omitted, as shown in the figure below.

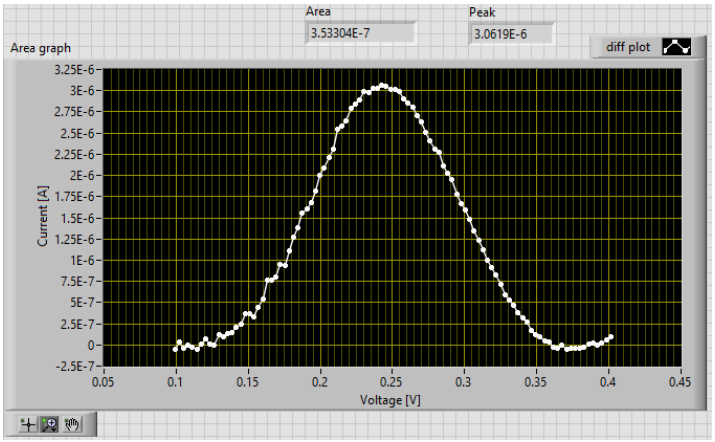

Figure 38. Result obtained with a fit selecting a reduced number of points. The curve obtained in this way is similar to the curves presented in Figure 33 - Figure 36 but a 3rd degree polynomial with a really small number of points have been used to calculate the baseline

Such method simplifies the process of baseline calculation. Indeed, by correctly choosing the range of points, it is possible to simplify the search for the optimal polynomial degree, shifting the choice from polynomials of high degree to polynomials of 3rd or 4th degree.

The method, however, has the not negligible disadvantage of the large number of parameters to be defined for an optimal fit, in fact in the first case there are three (upper and lower limit, degree of the polynomial) while in the second case there are five (upper and lower limit 1 and 2, degree of the polynomial) however in this second case the choice of the degree of the polynomial is of less importance by being able to keep it equal to 3 or 4. For this reason, starting from this result, we set out to develop techniques that could automate at least in part the setting of these parameters.

2.4.2 SEMI-AUTOMATIC METHOD

From now on, it was necessary to identify and compare the state of the art regarding automatic methods for baseline calculation. The literature is in fact quite rich in various more or less effective methods, being the problem of automatic calculation very common since proceeding manually usually requires a certain amount of time. Below I have presented the algorithms derived from the articles that I found most interesting.

Semi-automatic methods are characterized by the small number of parameters required to perform the baseline fit. Specifically, one can go on to define a completely new algorithm or define an

algorithm that, based on the manual multiparametric methods described earlier, goes on to define a criterion to automate the choice of values for these parameters. Specifically, two methods found in literature and applied to the topics of this thesis will be described. Starting then from these methods, more complex algorithms will be implemented with the aim of improving the results obtained. The first algorithm to be described is the one presented in the paper from Lukasz Gòrski et al. [24] . The algorithm involves defining two parameters: degree of the polynomial and number of iterations and it can be summarized with in Figure 39.

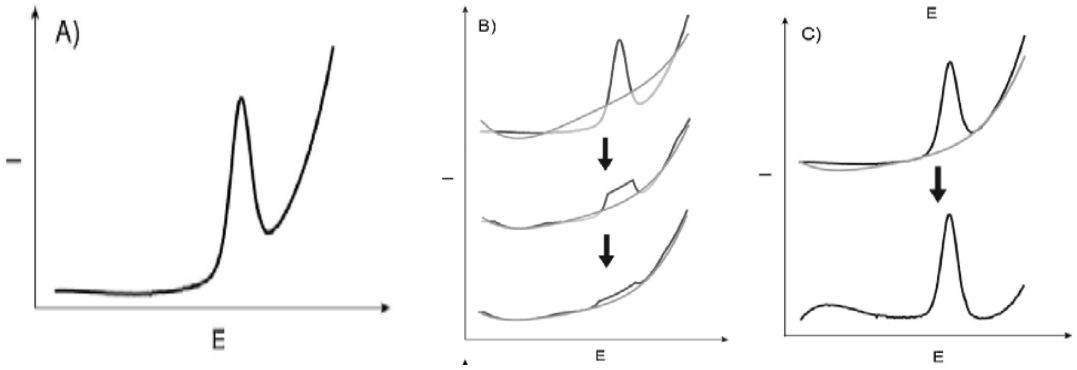

Figure 39. Step description [24]. A) Original DPV curve, B) Fit on the entire curve (upper), subtraction of the part of the DPV above the fit curve and fit of the resultant curve (mid plot), final fit of the resultant curve after n iterations. C) Original curve with baseline (upper), subtracted DPV curve (lower)

Starting from a DPV curve like the one defined in A). Having defined the above parameters, a polynomial fit is performed on the entire curve as described in the first curve in B). The part of the DPV curve that is greater than the fit curve will be cut off. This sequence of operations is performed for the defined number of iterations by performing at each subsequent iteration the polynomial fit on the curve that was not cut off in the previous iteration. At the end of the cycle of iterations the fit curve that is obtained corresponds to the baseline of the starting DPV curve as can be seen in C). The result of the baseline subtraction is represented in C).

The whole algorithm is reported in the following flowchart.

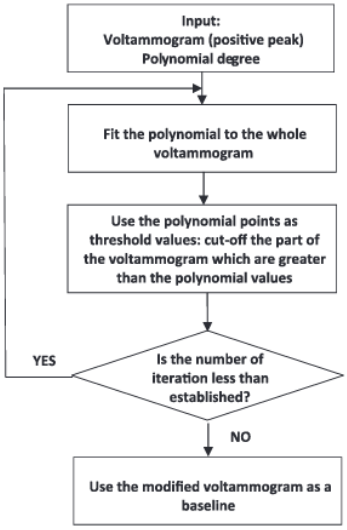

Figure 40. Flowchart of the algorithm [24]

For parameter definition, the authors suggest a number of iterations not less than 7 and to choose a value between 10 and 15. The choice of polynomial is a bit more complex. In this case it is possible to evaluate the FWHM (full width half maximum) of the curve. For narrower peaks (FWHM=12) we tend to use a polynomial of degree 5 or 6. While for wider peaks (FWHM=18) we recommend using polynomials of degree 2 or 3 [24].

Of course, this algorithm has been implemented and tested in LabVIEW. Here's an example. In Figure 41 the DPV curve on which building the baseline is represented.

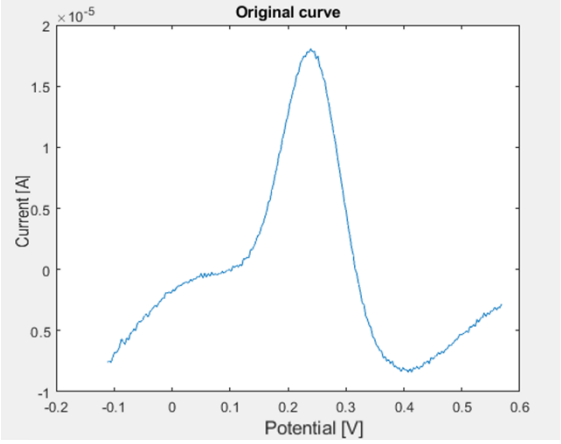

Figure 41. DPV curve used as example on which to calculate the baseline

We can see that it is a rather complex curve. I applied the algorithm using a number of iterations equal to 15 and a polynomial of 3rd degree. In the Figure 42 the result of the first iteration is reported.

The blue line represents the result of the fit on the entire curve, and the dashed line the part that is eliminated. The red curve is the remaining part (complementary to the dashed curve). The union obtained from the red curve and the blue curve will form a new curve on which at the next iteration the fit will be performed.

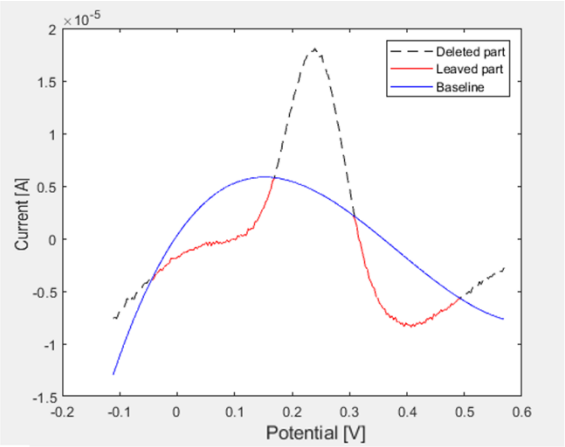

Figure 42. Result of the first iteration. Red curve+dashed curve represent the original DPV curve, blue curve is the baseline calculated on the entire curve on first iteration, the dashed curve is the part above the fit curve and in the next iteration will be eliminated, the red curve is the remaining part.

The algorithm goes on with this sequence of operations for another 14 iterations. The final result is shown in Figure 43.

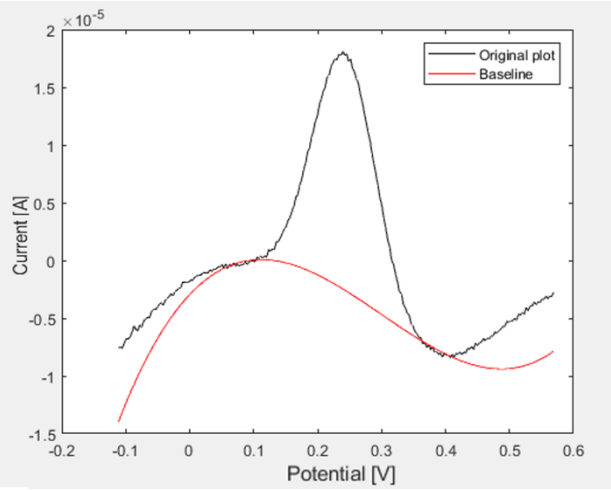

Figure 43. Final result. The result is quite good not considering the extremes of the DPV curve.

The result obtained in this way is correct. There are still errors at the extremes, but these can be negligible since extreme points of the curve are not informative about the electrochemical phenomena under evaluation so they can be deleted.

The algorithm can also work for complex DPV curves and using only two parameters, with the number of iterations kept constant at 15. It may lose in terms of computational complexity, but the algorithm is simple enough to not suffer much from an excessive number of iterations. The choice of the degree of the polynomial remains rather complex; in general, automating the choice of the value of this parameter can lead to serious errors in baseline tracking. Therefore, it would be appropriate to leave the optimal choice of the proper degree to the operator.

I did not find this method particularly effective. It works well for simpler curves like those presented in the article, but if you apply it to a more complex curve like the one that was used as an example in this thesis you can see how the algorithm struggles. The baseline is acceptable at the extremes between the peaks of interest but the extremes of the curve are not followed effectively by the baseline. From discussions with the research team at CNR, we realized that this is a minor problem and the algorithm was good enough as long as it was able to correctly select the points around the peak.

The second method serves as a transition between semi-automatic and automatic methods. In fact, it originates as a semi-automatic method that works with two parameters, but unlike the previous algorithm, the choice of values for these could be fully automated.

The algorithm is described on the paper by Xiao-Jun Tang et al. [25].

Although the paper refers to very different topics than those dealt with in this thesis and therefore the nature of the curves is particularly different, the methods used for constructing the baseline can also be applied to DPV curves. The method is based on least squares and specifically is a variation of it referred to as adaptive smoothness parameter penalty least squares (asPLS).

Without going into the specifics of the mathematical method, the flowchart used to implement the algorithm is presented in Figure 44.

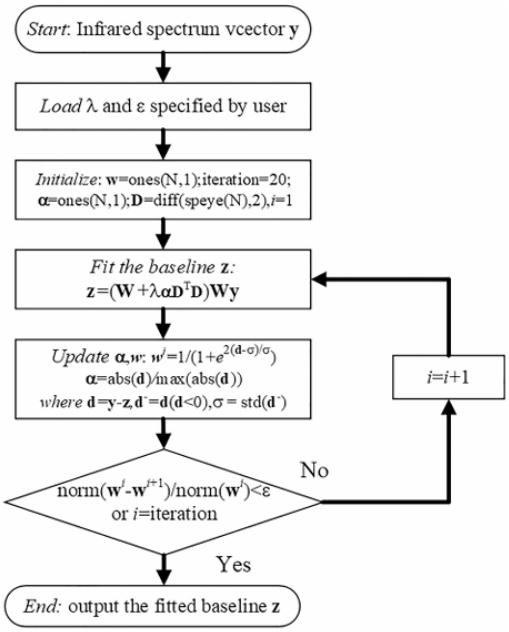

Figure 44. Flux diagram asPLS [25]

At first a value of λ and ε is specified. These are the only two parameters required. The variables defined in the third step are initialized. Now starts a while loop in which at each iteration a fit of the DPV curve is performed using the weighted least squares. A trace is kept of the evolution of the weights at each iteration because the output of the loop is governed by the difference of the weights between the current iteration and the previous iteration. To avoid loops or an excessive number of iterations in the case the algorithm does not converge to a solution, a maximum value "iteration" of iterations is set. The choice of introducing weights into the algorithm is particularly efficient because it allows to not consider all points on the DPV curve of "equal importance" for the fit. In fact, the main disadvantage of the algorithms described previously consists precisely in the fact that all points weigh equally in the calculation of the fit, but for the purpose of the fit of the baseline it is known that it is necessary to rely more on some points than on others. See in fact the algorithm described in the manual method, which involves selecting these points as accurately as possible, leaving out points outside the range of interest.

The algorithm was then tested on the DPV curves obtained from the measurements taken. The Figure 45 shows the result obtained on the curve shown in red with the subsequent subtraction of the baseline.

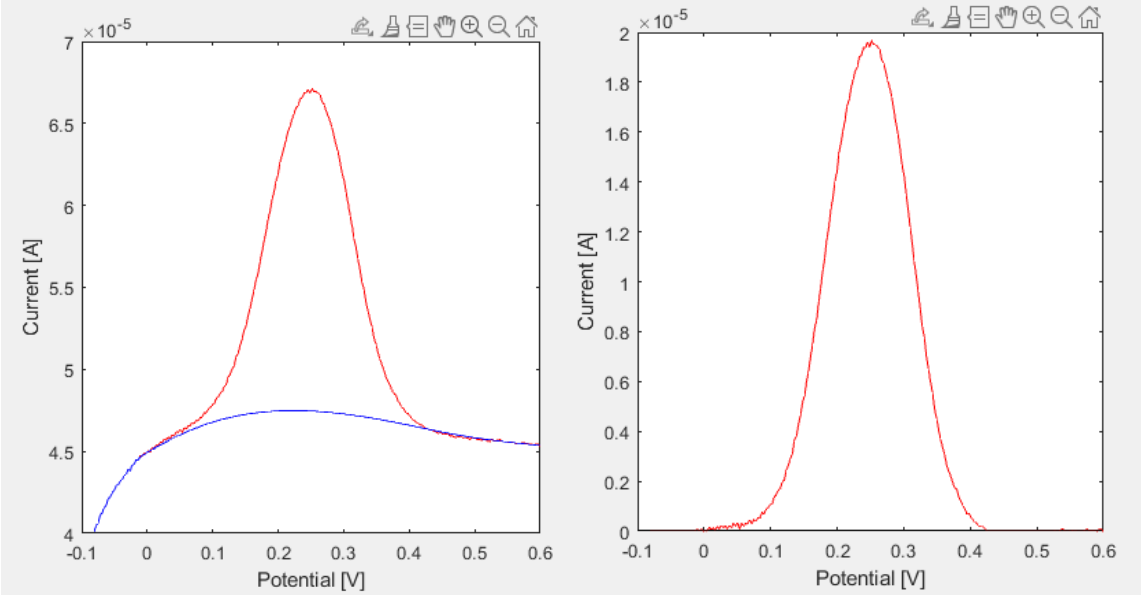

Figure 45. Result obtained with asPLS method. $\Lambda=10^7$, $\varepsilon=10^{-4}$

This last algorithm was quite complex to understand but I found it particularly efficient. It uses mathematical concepts such as the use of weights and least squares, which I identified as the ideal methods for developing a more robust algorithm. I think it is interesting that this method was taken from an article that focuses on the problem of baseline computation on particularly complex and noisy signals (developed for the infrared spectra case study). So as far as the article did not deal with DPV curves (the subject of our study), it proposed an effective method for baseline calculation for proceeding in this thesis as well.

2.4.3 AUTOMATIC METHOD

As already mentioned, the automatic method developed here is based on the asPLS method presented earlier. This is a method I implemented and developed after observing the curves obtained from the first measurements by performing several tests, inspired by the methods described above.

The small number of parameters required and the relative simplicity of assigning a value to them makes this method suitable for automation. Starting with parameter ε, this is used to quantify the minimum deviation between the values that the weights have between one iteration and the next. When this deviation is sufficiently small, i.e. less than ε, then the algorithm ends its while cycle. This means that between the two fits of the baseline obtained in the current iteration and the

previous one there is a negligible difference, so the fit obtained in the current iteration can be considered as the final result. The value of ε can therefore be considered fixed and sufficiently small, so it was deemed sufficient to keep it constant at a value of 10^{-4}.

Once this consideration has been made, the only parameter to be automated is λ. This is called the smoothing parameter and is intended to quantify how closely the fit curve should "follow" the original curve. This means that higher λ values will result in a fit that follows the original curve less closely (a more "rigid" curve), whereas lower λ values will have the opposite effect. Using the asPLS method it is also possible to make this parameter flexible by varying it according to the position on the DPV curve. In fact, one would like the λ parameter to be higher in the peak region while lower in the regions to the sides. This can be done by introducing an α parameter defined as:

$$\alpha = \frac{|\, y_i - z_i \,|}{\max(|\, y_i - z_i \,|)}$$

Where y_i is the original curve and z_i is the fitted curve at the current iteration. Thus, α quantifies the distance between the two curves point by point thus will take on larger values at points around the peak zone and smaller or zero values around the regions on the sides. For this reason, it is useful to multiply this parameter by λ to guarantee this type of flexibility when performing the fit. At this point the choice of lambda becomes less complex because the algorithm is able to identify and evaluate the different points of the DPV curve appropriately. The parameter takes on values of exponents of 10 and the authors suggest keeping it in the power range between 4 and 8. In the specific case of the work in this thesis and after several measurements on real samples, it was noticed that the optimum value of the exponent of this parameter is always 6 or 7. The difference in the choice lies in the complexity of the curve being considered. By referring to the algorithm described in [24], it is possible to quantify the level of complexity of the curve by evaluating the amplitude of the peak region, i.e. the FWHM. For this reason, a power of 6 will be used for curves with wider peaks, and a power of 7 for curves with narrower peaks. Here we have two examples.

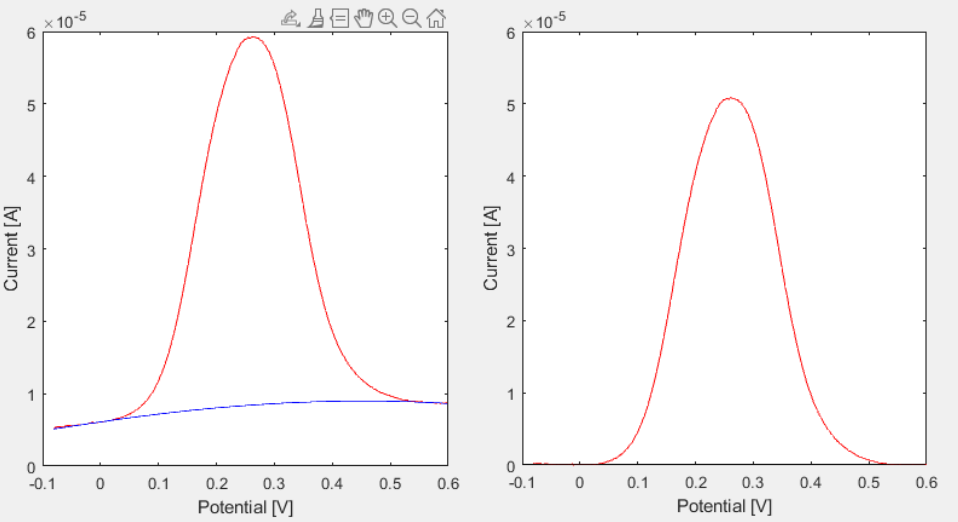

Figure 46. Differential Pulse Voltammetry with ferricyanide PBS using a flat platinum electrode on which have been deposited short carbon nanotubes and (poly)pyrrole 0.25 M with a 10 cycles cyclic voltammetry deposition. Concentration: 5uM. λ = 7.

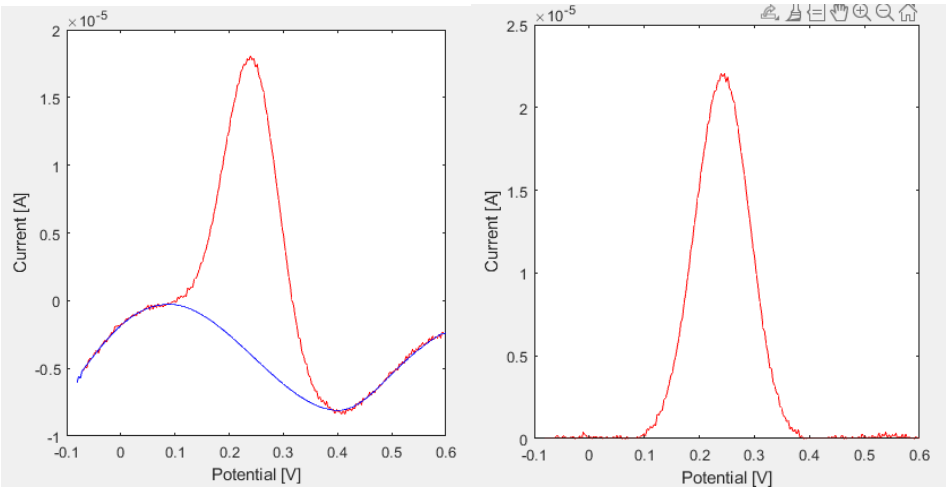

Figure 47. Differential Pulse Voltammetry with ferricyanide PBS using a flat platinum electrode on which have been deposited a film of cork (0.1 mg/mL) and (poly)pyrrole 0.25 M with a 10 cycles cyclic voltammetry deposition. λ = 6. 8

3. CHAPTER 3: RESULTS

Up to this point, the work presented has been almost solely engineering in terms of software and electronics design. The next phase is the phase of testing. A case study is presented in which the system I have built can be of particular interest because of the advantages it shows. First, its proper functioning and applicability to real case studies can be demonstrated. With the help of Dr. Giulia Siciliano, I then began the actual testing and measurement phase with the ultimate goal of providing optimal results.

3.1. LABVIEW AND NOVA MEASUREMENT COMPARISON

The first part of Result Chapter includes the tests performed on measurements acquired previously to verify the correct functioning of the application and the correct data acquisition.

I was then provided with microelectrodes on which a film of poly-pyrrole or aniline was electro-deposited and I have performed measurements by placing on them a drop of electrolyte solution. Below is the detail.

3.1.1. MEASUREMENTS DESCRIPTION

The electro-co-deposition of a film of composite material containing cork and polypirrole (Cork-Ppyrr) was obtained on single-use platinum microelectrodes patterned on glass substrates by cyclic voltammetry (CV, 10 scans) in the potential range −0.2 – 0.8 V vs. Ag/AgCl at a scan rate of 20 mV s−1 in an aqueous solution containing 0.25 M pyrrole and 0.1 mg/mL cork-Ppyrr.

I performed the same method of deposition on other microelectrodes by replacing pyrrole with 0.25M aniline in HCl.

The control electrodes marked as “pani” or “pyrr”, were obtained in the same way without cork being added to the solution.

I have used the following microelectrodes for testing the measurements (in parentheses the plots of the next pages they refer to):

- Pyrrole [plot (A)]
- Polyaniline [plot (B)]
- Cork- pyrrole [plot (C) and (D)]
- Cork- polyaniline [plot (E) and (F)]

The measurements carried out in this phase consist of:

- Cyclic voltammetry with ferricyanide in PBS (10 mM $K_3[Fe(CN)_6]/K_4[Fe(CN)_6]$ (1 : 1))
- Differential pulse voltammetry with ferricyanide in PBS (10 mM $K_3[Fe(CN)_6]/K_4[Fe(CN)_6]$ (1 : 1))
- Cyclic voltammetry with ruthenium (2 mM) in PBS
- Cyclic voltammetry with PBS

In order to obtain the most accurate verification possible, I carried out CV and DPV measurements in sequence by using at first the application designed on LabVIEW and then the Nova software. To better compare the measurements, I have of course taken sequentially (i.e. few seconds later), not modifying the position of the electrodes or the drop on the flat electrode.

On each microelectrode I have performed CV and DPV measurements by using different redox probes, in particular ferricyanide in PBS and ruthenium in PBS, cyclic voltammetry with PBS only, and differentiated pulsatile voltammetry with ferricyanide PBS. I performed each measurement first using LabVIEW and then NOVA program.

This step did not give any particular problems, it was only necessary to make sure that the measurement setup was done correctly. For example, I had to pay attention to the placement of the electrodes, which must not touch each other but which must be in contact with the drop, the drop then must not spill out of the surface where it was placed or even come into contact with the alligator clips. After a few clumsy attempts, I managed to gradually become more and more familiar and precise.

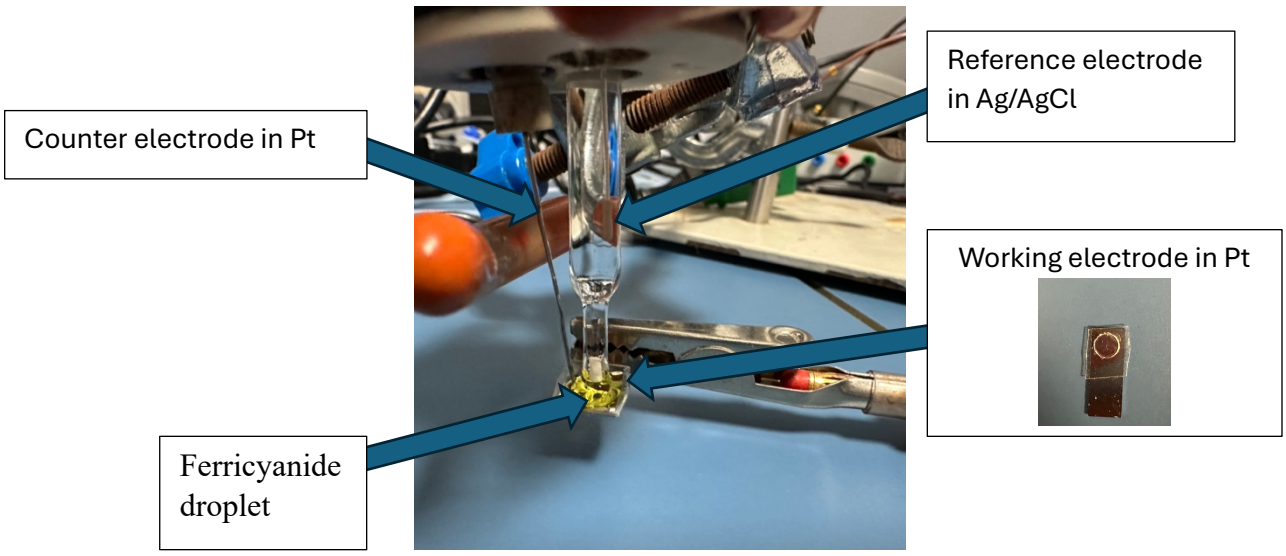

Figure 48. Measurement setup, the position of the droplet on the Working electrode is demarcated with pierced tape

The representation of these results is divided into four sections according to the type of measurement performed. For each, selected figures are shown for visual comparison and the numerical results of all measurements are presented in a table.

3.1.2. QUANTITATIVE AND QUALITATIVE DATA COMPARISON

3.1.2.1. Cyclic voltammetry with ferricyanide in PBS

The setup parameters entered in the procedure for this type of measurement are listed below.

- Command name: CV staircase
- Start Potential: -0.6 V
- Upper Vertex Potential: 0.6 V
- Lower Vertex Potential: -0.6 V
- Stop Potential: -0.008 V
- Number of scans: 3
- Scan rate: 0.1 V/s
- Step: 0.00244 V

The following images show some visual comparisons.

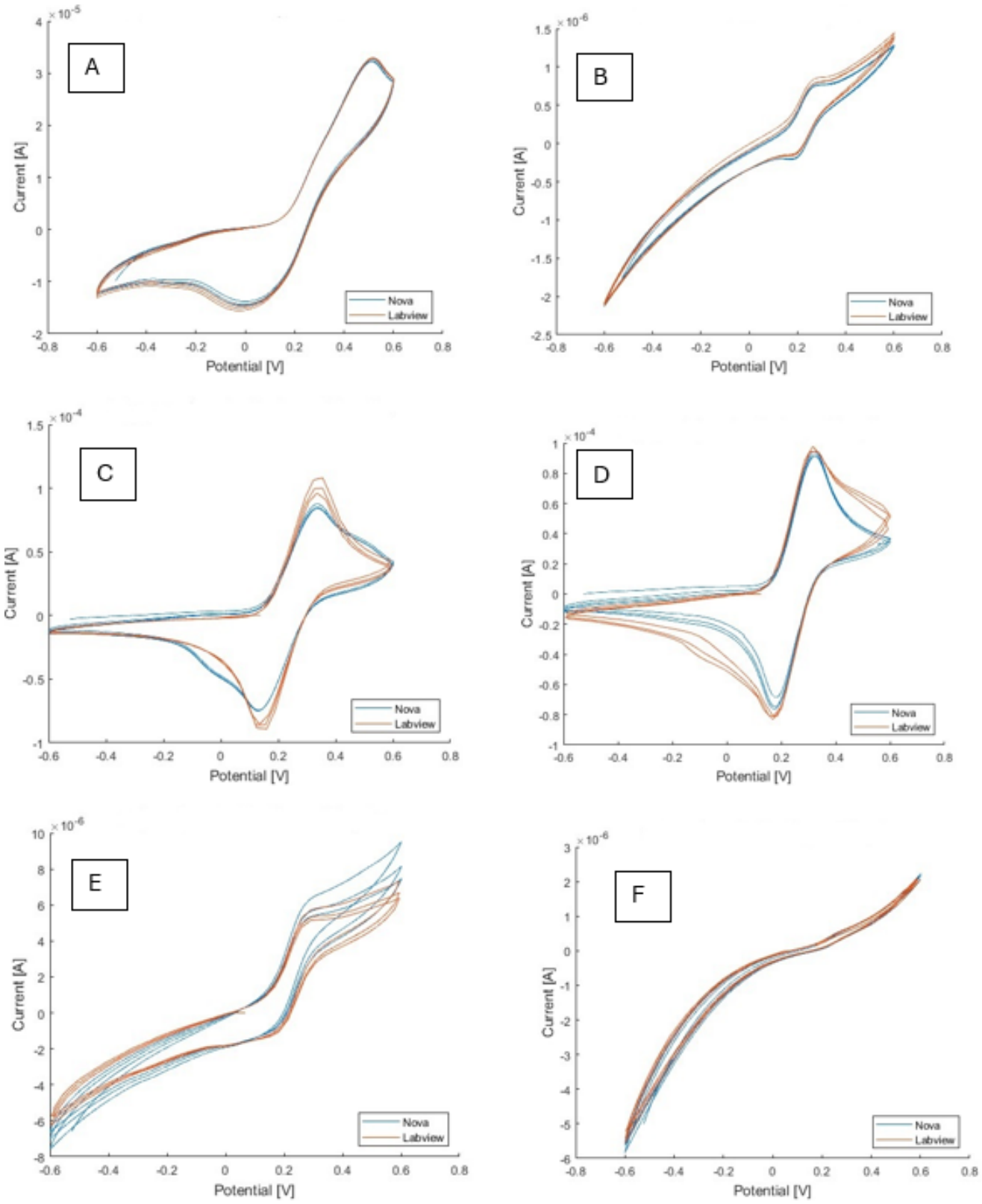

Figure 49. Visual comparison of measurements taken with LabVIEW (red) and Nova (blue) (Applied Voltage on x-axis vs Current on y-axis). CV graphs of: A) Ppyrr film; B) Pani film; C) and D) Cork- ppyrr composite; E) and F) Cork- pani composite

Below have a table sum up the comparison between the two methods from a quantitative point of view.

	NOVA		LABVIEW	
	Area $[A \cdot V]$	**Peak Current [A]**	**Areaù $[A \cdot V]$**	**Peak Current [A]**
pyrrol cv ferricyanide PBS (A)	2.62×10^{-5}	5.11×10^{-1}	2.62×10^{-5}	5.16×10^{-1}
pani cv ferricyanide PBS (B)	4.23×10^{-8}	3.00×10^{-1}	4.25×10^{-8}	2.98×10^{-1}
Cork- ppyrr cv ferricyanide PBS (C)	8.02×10^{-5}	3.35×10^{-1}	1.05×10^{-4}	3.55×10^{-1}
Cork- ppyrr cv ferricyanide PBS (D)	9.09×10^{-5}	3.20×10^{-1}	9.25×10^{-5}	3.16×10^{-1}
Cork- pani cv ferricyanide PBS (E)	4.40×10^{-6}	2.70×10^{-1}	4.00×10^{-6}	2.91×10^{-1}
Cork- pani cv ferricyanide PBS (F)	2.42×10^{-7}	2.69×10^{-1}	2.40×10^{-7}	2.67×10^{-1}

Table 1. Quantitative comparison on measures taken.

	DIFFERENCE	
	Area $[A \cdot V]$	**Peak Current [A]**
pyrrol cv ferricyanide PBS (A)	3.15×10^{-8}	5.34×10^{-3}
pani cv ferricyanide PBS (B)	1.52×10^{-10}	2.00×10^{-3}
Cork- ppyrr cv ferricyanide PBS (C)	2.46×10^{-5}	1.99×10^{-2}
Cork- ppyrr cv ferricyanide PBS (D)	1.57×10^{-6}	4.55×10^{-3}
Cork- pani cv ferricyanide PBS (E)	3.98×10^{-7}	2.10×10^{-2}
Cork- pani cv ferricyanide PBS (F)	2.23×10^{-9}	2.00×10^{-3}

Table 2. Difference between the two measures

The average difference with the standard deviation was then calculated, so we have:

- Area: $4.44\times10^{-6} \pm 2.20\times10^{-7}$
- Peak current: $9.14\times10^{-3} \pm 4.57\times10^{-4}$ A

To conclude, the maximum percentage error that can be obtained during measurement was then calculated and this corresponds to 4.57%.

We now move on to a comparison of the DPV measurements obtained with Nova and LabVIEW.

3.1.2.2. Differential pulse voltammetry with ferricyanide in PBS

The setup parameters entered in the procedure for this type of measurement are listed below.

- Command name: Differential pulse
- Start potential: -0.2 V
- Stop potential: 0.6 V
- Step: 0.003
- Modulation amplitude: 0.025
- Modulation time: 0.02
- Interval time: 0.03

In the following page.

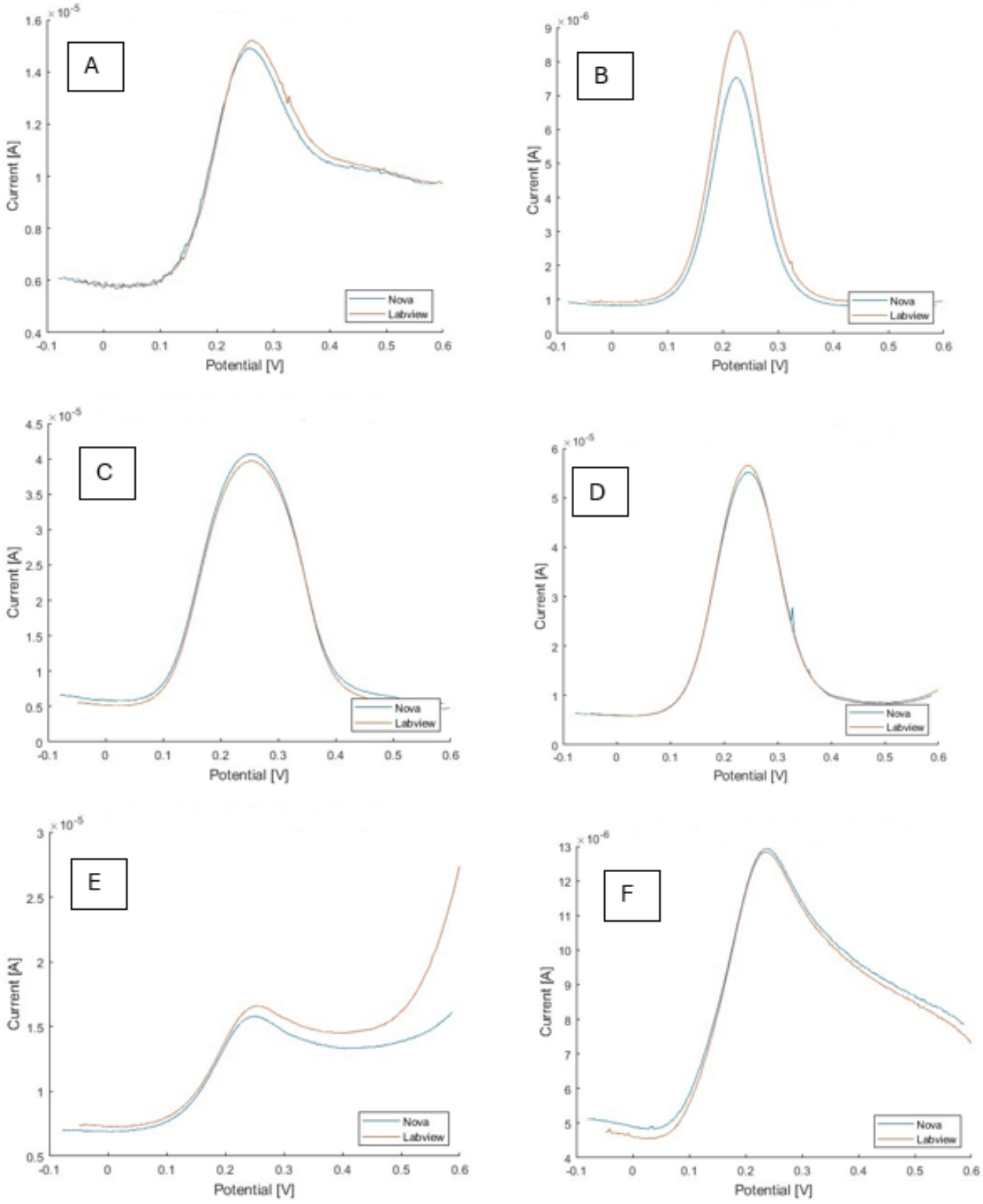

Figure 50. *Visual comparison of measurements taken with LabVIEW (red) and Nova (blue) (Applied Voltage on x-axis vs Current on y-axis). DPV graphs of: A) Ppyrr film; B) Pani film; C) and D) Cork- ppyrr composite; E) and F) Cork- pani composite*

Below have a table sum up the comparison between the two methods from a quantitative point of view.

	NOVA			LABVIEW		
	Area $[A \cdot V]$	**Peak Current [A]**	**Peak Current position [V]**	**Area $[A \cdot V]$**	**Peak Current [A]**	**Peak Current position [V]**
pyrrol DPV ferricyanide PBS (A)	8.86×10^{-7}	6.30×10^{-6}	0.254	9.11×10^{-7}	6.48×10^{-6}	0.257
pani DPV ferricyanide PBS (B)	7.63×10^{-7}	6.68×10^{-6}	0.224	9.27×10^{-7}	7.94×10^{-6}	0.227
Cork- ppyrr DPV ferricyanide PBS (C)	6.11×10^{-6}	3.32×10^{-5}	0.25	6.22×10^{-6}	3.34×10^{-5}	0.25
Cork- ppyrr DPV ferricyanide PBS (D)	6.67×10^{-6}	4.72×10^{-5}	0.245	6.80×10^{-6}	4.88×10^{-5}	0.245
Cork- pani DPV ferricyanide PBS (E)	9.47×10^{-7}	5.92×10^{-6}	0.242	8.56×10^{-7}	5.73×10^{-6}	0.245
Cork- ppyrr DPV ferricyanide PBS (F)	1.07×10^{-6}	5.45×10^{-6}	0.23	1.01×10^{-6}	5.49×10^{-6}	0.224

Table 3. Quantitative comparison on measures taken

	DIFFERENCE		
	Area [A · V]	**Peak Current [A]**	**Peak Voltage position [V]**
pyrrol DPV ferricyanide PBS (A)	2.48×10^{-8}	1.81×10^{-7}	3×10^{-3}
pani DPV ferricyanide PBS (B)	1.64×10^{-7}	1.25×10^{-6}	3×10^{-3}
Cork- ppyrr DPV ferricyanide PBS (C)	1.07×10^{-7}	2.00×10^{-7}	0
Cork-ppyrr DPV ferricyanide PBS (D)	1.21×10^{-7}	1.53×10^{-6}	0
Cork- pani DPV ferricyanide PBS (E)	9.10×10^{-8}	1.89×10^{-7}	3×10^{-3}
Cork- pani DPV ferricyanide PBS (F)	5.56×10^{-8}	3.56×10^{-8}	6×10^{-3}

Table 4. Difference between the two measures

The average difference with the standard deviation was then calculated, so we have:

- Area: $9.40\times10^{-8} \pm 3.76\times10^{-9}$
- Peak current: $5.65\times10^{-8} \pm 2.26\times10^{-9}$ A
- Peak Voltage position: $2.50\times10^{-3} \pm 1.00\times10^{-4}$ V

To conclude, the maximum percentage error that can be obtained during measurement was then calculated and this corresponds to 4.03%.

3.1.2.3. Cyclic Voltammetry with ruthenium in PBS

As usual the setup parameters entered in the procedure for this type of measurement are listed below.

- Command name: CV staircase
- Start potential: -0.8 V
- Upper vertex potential: 0.4 V
- Lower vertex potential: -0.8 V
- Stop Potential: -0.008 V
- Number of scans: 3
- Scan rate: 0.1 V/s
- Step: 0.00244

Below we have some comparisons.

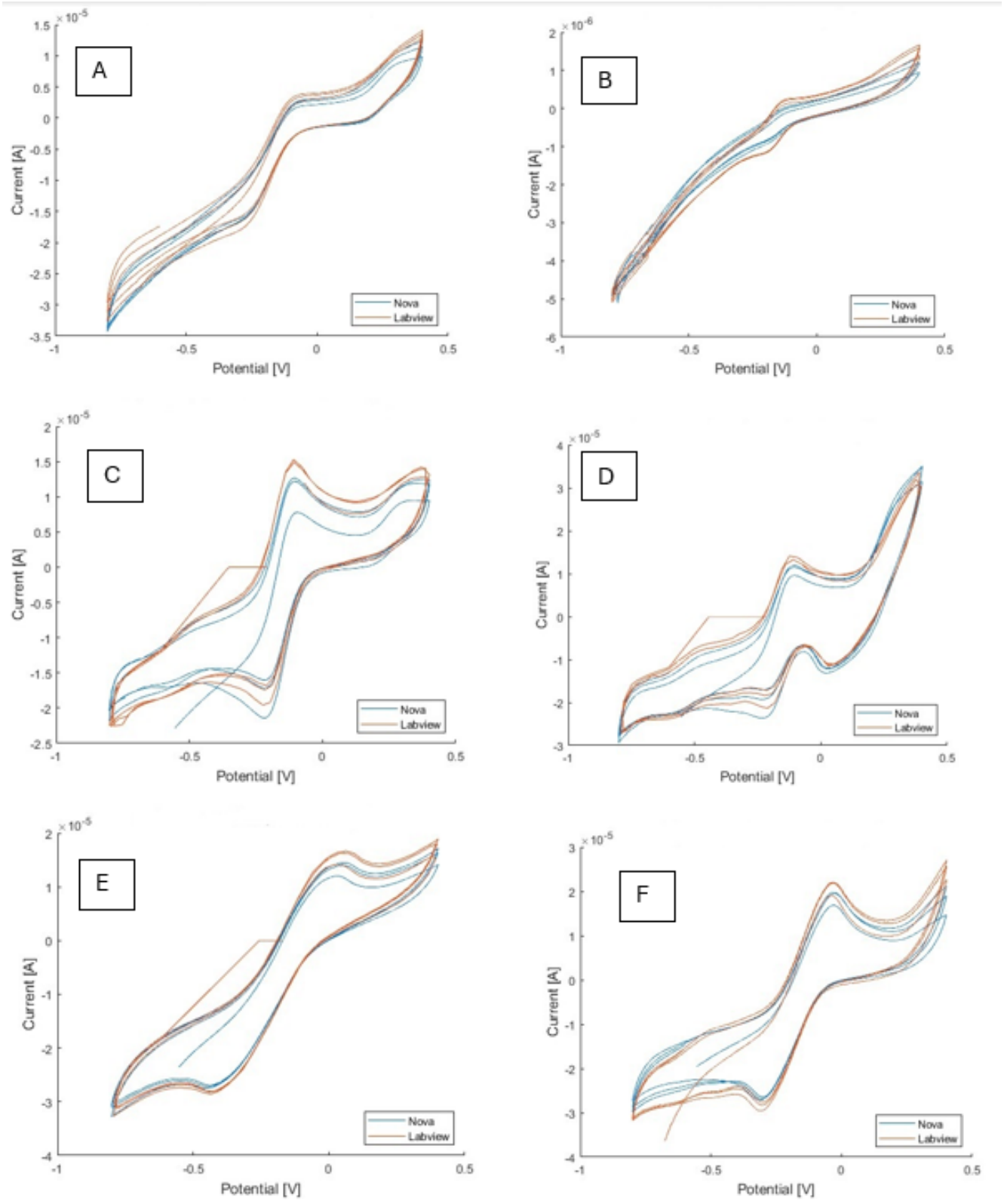

Figure 51. *Visual comparison of measurements taken with LabVIEW (red) and Nova (blue) (Applied Voltage on x-axis vs Current on y-axis). CV graphs of: A) Ppyrr film; B) Pani film; C) and D) Cork- ppyrr composite; E) and F) Cork- pani composite*

Here we have the quantitative comparison.

	NOVA		LABVIEW	
	Area $[A \cdot V]$	**Peak Current [A]**	**Area $[A \cdot V]$**	**Peak Current [A]**
pyrrol cv ruthenium PBS (A)	9.24×10^{-6}	-9.00×10^{-2}	1.03×10^{-5}	-9.40×10^{-2}
pani cv ruthenium PBS (B)	6.48×10^{-8}	-1.40×10^{-1}	6.37×10^{-8}	-1.60×10^{-1}
Cork- ppyrr cv ruthenium PBS (C)	1.36×10^{-5}	-1.04×10^{-1}	1.63×10^{-5}	-1.09×10^{-1}
Cork- ppyrr cv ruthenium PBS (D)	1.48×10^{-5}	-1.10×10^{-1}	1.60×10^{-5}	-1.05×10^{-1}
Cork- pani cv ruthenium PBS (E)	1.75×10^{-5}	4.70×10^{-2}	1.76×10^{-5}	4.10×10^{-2}
Cork- pani cv ruthenium PBS (F)	1.68×10^{-5}	-2.60×10^{-2}	1.88×10^{-5}	-2.40×10^{-2}

Table 5. Quantitative comparison on measures taken

	DIFFERENCE	
	Area $[A \cdot V]$	**Peak Current [A]**
pyrrol DPV ruthenium PBS (A)	1.10×10^{-6}	4.00×10^{-3}
pani DPV ruthenium PBS (B)	1.11×10^{-9}	2.00×10^{-3}
Cork- ppyrr cv ruthenium PBS (C)	2.69×10^{-6}	4.79×10^{-3}
Cork- ppyrr cv ruthenium PBS (D)	1.18×10^{-6}	-5.00×10^{-7}
Cork- pani cv ruthenium PBS (E)	1.63×10^{-7}	6.00×10^{-3}
Cork- pani cv ruthenium PBS (F)	2.00×10^{-6}	-2.00×10^{-3}

Table 6. Difference between the two measures

The average difference with the standard deviation was then calculated, so we have:

- Area: $1.19\times10^{-6} \pm 9.52\times10^{-8}$
- Peak current: $4.63\times10^{-3} \pm 3.7\times10^{-4}$ A

To conclude, the maximum percentage error that can be obtained during measurement was then calculated and this corresponds to 8.06%.

3.1.2.4. Cyclic Voltammetry in PBS

The setup parameters entered in the procedure for this type of measurement are listed below.

- Command name: CV staircase
- Start potential: -0.6 V
- Upper vertex potential: 0.6 V
- Lower vertex potential: -0.6 V
- Stop Potential: -0.06 V
- Number of scans: 3
- Scan rate: 0.05 V/s
- Step: 0.00244

In this case, only images will be presented to allow a visual comparison. From cyclic voltammetry in PBS, the presence of quantifiable peaks is not to be expected; generally, this type of measurement is carried out to verify the stability of the deposition.

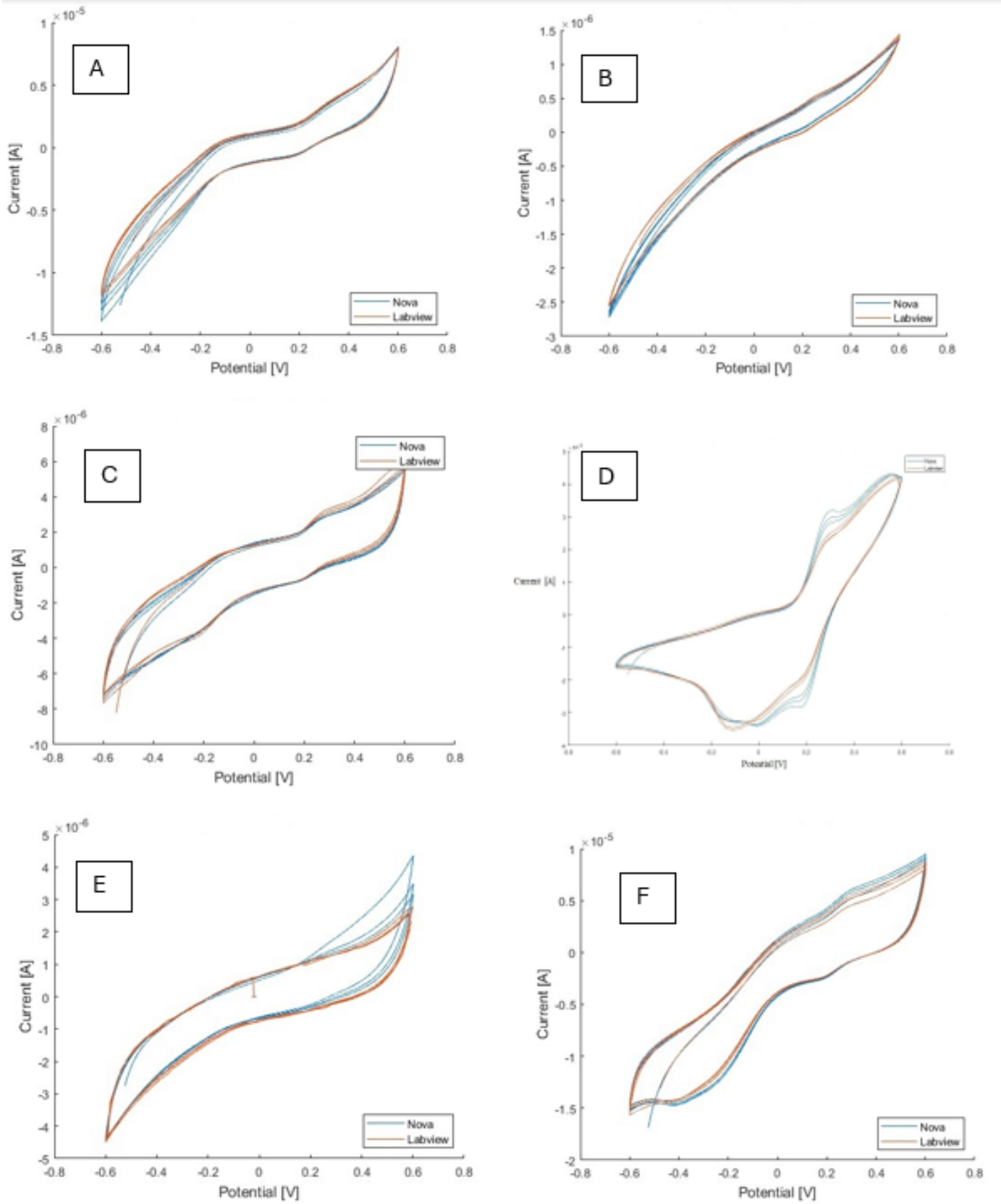

Figure 52. *Visual comparison of measurements taken with LabVIEW (red) and Nova (blue) (Applied Voltage on x-axis vs Current on y-axis). CV graphs of: A) Ppyrr film; B) Pani film; C) and D) Cork- ppyrr composite; E) and F) Cork- pani composite*

3.2. SYNTHESIS AND CHARACTERIZATION OF *CYROMAZINE* MIP RECEPTOR

3.2.1. CARBON NANOTUBES FILM WITH *CYROMAZINE* DEPOSITION AND TEST

The following depositions were made with the help of Dr. Giulia Siciliano. Not having sufficient chemistry background to make the described compounds, I joined her work and the subsequent tests were carried out with her supervision.

The electro-co-deposition of the (poly)pyrrole–Carbon Nanotubes (PPyrr-CNTs) composite film was carried out on single-use platinum microelectrodes patterned on glass substrates by cyclic voltammetry (CV) (5-10 scans) in the potential range −0.2 – 0.8 V vs. Ag/AgCl at a scan rate of 20 mV s−1 in aqueous solution of 0.25 M pyrrole and 0.3 mg/mL CNTs, containing *cyromazine* at a concentration of 6µM.

The composite film was formed on the electrode surface by using 5 or 10 cycles of CV (in both cases one monitored by LabVIEW software and the other one monitored by NOVA), for a total of 4 depositions.

Figure 53 reports typical cyclic voltammogram (10 scans) recorded during the electro-polymerization of PPyrr-CNTs in the presence of *cyromazine* on platinum electrodes. An increase in the anodic peak was observed from the 1st to the 10th cycle, indicating the formation of the conductive polymer film on the electrode surface.

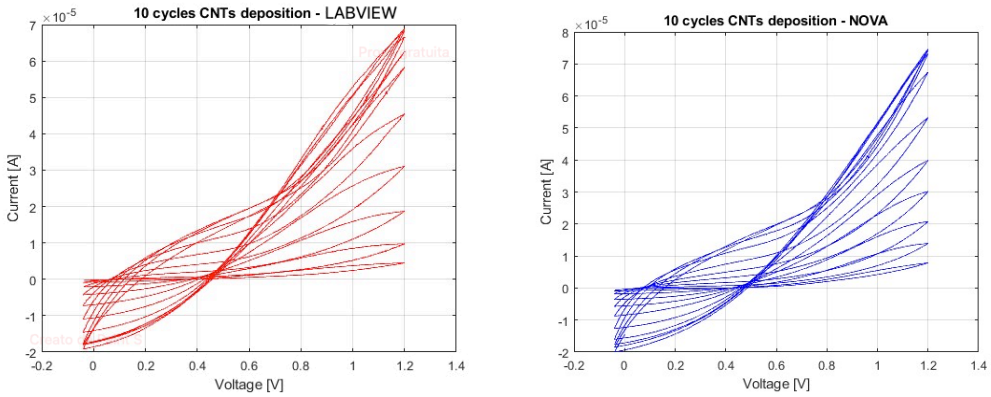

Figure 53. Cyclic voltammogram (10 scans) recorded during the electro-polymerization of PPyrr-CNTs (0.25 M pyrrole and 0.3 mg/mL CNTs) in the presence of cyromazine on platinum electrodes. In red the one recorded by LabVIEW and in blue the one recorded by NOVA.

CV measurements were carried out in ferricyanide in PBS to verify peak height and position, while CV measurements in PBS were performed to assess the stability of the synthetized film.

For each test, I have made a comparison between the results obtained by using 5 and 10 scans deposition and, at the same time, I compared the data obtained by using the same deposition protocol (these were differentiated as 'LabVIEW' and 'NOVA' according to the software used to collect the deposition data, keeping in mind that the protocol is the same, so similar results are expected in this case). Figure 54 reports a comparison on CV measurements performed on two different devices where the electro-polymerization of Ppyrr-CNTs composite (10 scans) was carried out.

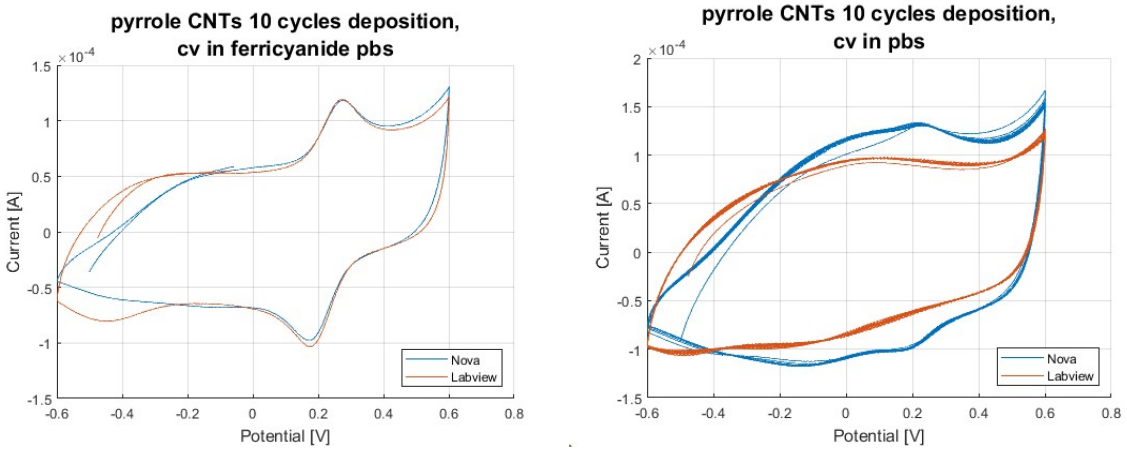

Figure 54. Figure 55. Visual comparison of the two devices obtained with a 10 scans deposition. On the top a cyclic voltammetry with ferricyanide PBS, on the bottom cyclic voltammetry with PBS, 10 scans (Area_LabVIEW=0.0688, Area_NOVA=0.0812).

Visually, it can be seen from the CV in ferricyanide that the peaks coincide in position and height. The CV measurements performed in PBS highlight that both devices pass the stability test and the cycles overlap each other, however there is a difference between the calculated areas, this means indicating the two devices do not appear to be perfectly identical.

Below we have a quantitative comparison of the peak voltage and peak current in the cyclic voltammetry with ferricyanide.

	Peak current [A]	Peak voltage [V]
LabVIEW	1.92×10^{-5}	0.245
NOVA	1.87×10^{-5}	0.242

Table 7. Quantitative comparison on 10 cycles deposition

A more interesting result can be seen following a comparison between devices obtained by using different cylcles of deposition (5 cycles and 10 cycles).

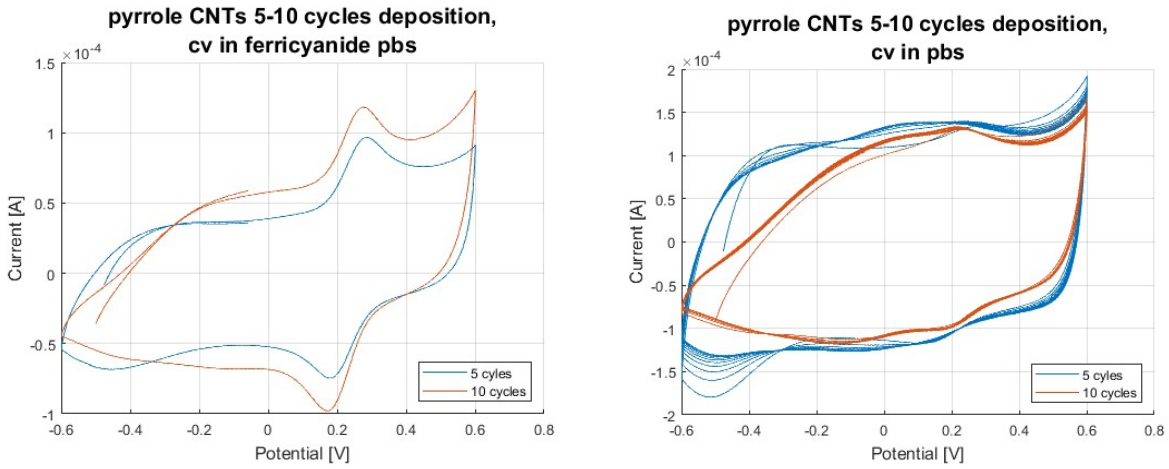

Figure 56. Figure 57. Visual comparison of cyclic voltammetries obtained from 5-10 cycles depositions. In green the 5 cycles deposition, in purple the 10 cycles deposition.

Visually we can notice that the peak referred to the 5 cycles deposition is in the same position respect to that at 10 cycles but the height is slightly lower. It is now possible to make a quantitative comparison.

Below we have a quantitative comparison of the peak voltage position and the peak current intensity recorded by CV in ferricyanide and a quantitative comparison of the areas of the CV curves in PBS.

	Peak current [A]	Peak voltage [V]
5 scans	1.58×10^{-5}	0.239
10 scans	1.87×10^{-5}	0.242

Table 8. Quantitative comparison on 5-10 cycles deposition

	Area $[\boldsymbol{A}\cdot\boldsymbol{V}]$
5 scans	0.1066
10 scans	0.0812

Table 9. Quantitative comparison of the Areas on 5-10 cycles deposition

As could be visually guessed, the peak height in the 5 cycles deposition is slightly lower than in the 10 cycles and the difference is of 0.29×10^{-5}, resulting in a thicker and more insulating film on the platinum microelectrode than the film deposited on the 10-cycle electrode.

3.2.2. ELECTRO-CO-DEPOSITION OF THE (POLY)PYRROLE–CARBON NANOTUBES

In this final section I have reported the synthesis and electrochemical characterization of a MIP-based sensor for *cyromazine* detection. The aim is to understand the possible electroactive properties of *cyromazine* and monitor the current peak changes by varying the concentration. As mentioned above, single-use platinum microelectrodes were used to deposit a film of (poly)pyrrole–Carbon Nanotubes (PPyrr-CNTs) by cyclic voltammetry (CV) (5-10 scans) in the potential range −0.2 – 0.8 V vs. Ag/AgCl at a scan rate of 20 mV s−1 in aqueous solution of 0.25 M pyrrole and 0.3 mg/mL CNTs, containing *cyromazine* at a concentration of 6µM.

After polymerization, the modified electrode was washed with a solution of acetic acid 5% for template removal. The DPV results of imprinted electrodes before and after template removal carried out in the presence of 10 mM $K_3[Fe(CN)_6]/K_4[Fe(CN)_6]$ (1 : 1) at room temperature show that the washing step with the solution of acetic acid 5% increases the peak current and leads to an effective release of the template, thus favoring the electron transfer between the solution and the electrode.

Then, to further investigate the MIP-*cyromazine* binding and evaluate the sensing performance, I have incubated the biosensors with binding buffer solution containing increasing concentrations of cyromazine, ranging from 1.5 to 5 µM, for 1 hour; then, a washing step was performed. DPV was used to monitor the ferri/ferrocyanide probe response as affected by *cyromazine* binding on the MIP-receptor. Data reported in Figure 58 and Figure 59 show DPV graphs after incubation with *cyromazine* at different concentrations. The rebinding test with *cyromazine* at increasing concentrations show an increase of redox peak currents of the ferri/ferrocyanide couple with increasing *cyromazine* concentration, thus suggesting an electroactive behavior of the template molecule.

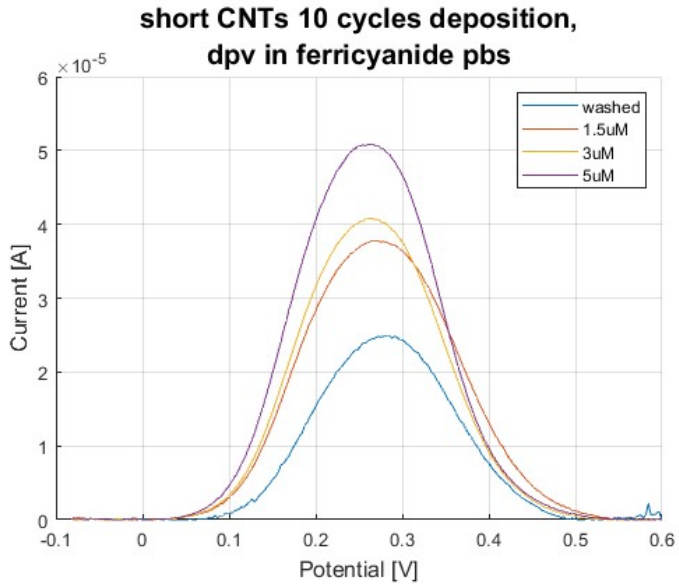

Figure 58. *DPV curves showing the directly proportional peak increase as the concentration increases. Short Carbon Nanotubes were used for the electro-co-deposition.*

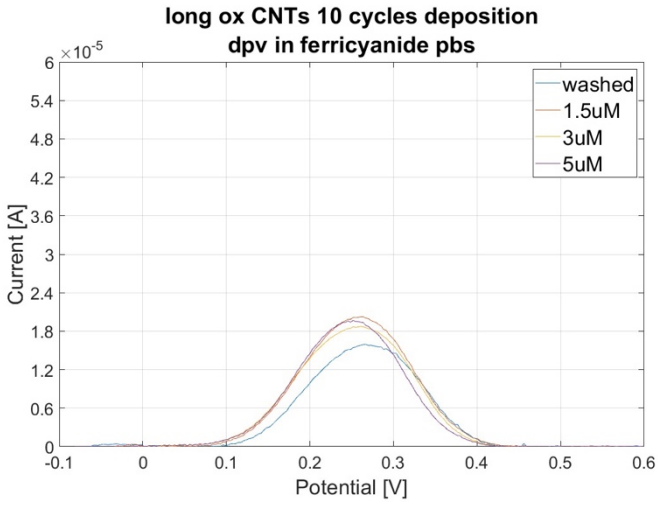

Figure 59. DPV curves showing the directly proportional peak increase as the concentration increases. Long Carbon Nanotubes (long-cnts) were used for the electro-co-deposition. Note how the linearity of the trend between concentration and peak height seems to be lost compared to the short-cnts. There is no particular difference in height between 1.5 and 3 uM

The calibration plot, constructed by plotting the MIP current intensities normalized with respect to the washed MIP current intensity as a function of the logarithm of *cyromazine* concentration, displayed a linear response in the tested concentration range (Figure 60).

These preliminary results suggest that the novelty of the MIP-based approach relies on the fact that the developed miniaturized sensor for *cyromazine* is sensitive and selective, since it can detect *cyromazine* at low concentrations. The experimental results open the way to quantitative measurements of *cyromazine* concentration in biological samples upon further calibration and specificity tests to be carried out in presence of possible interferents.

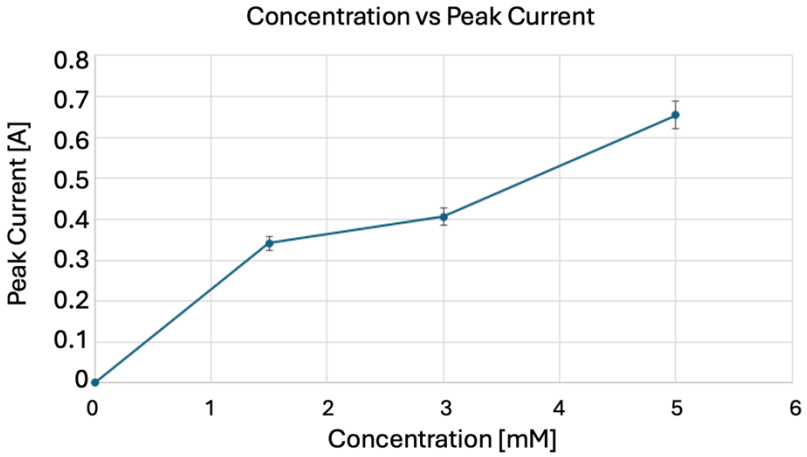

Figure 60. Calibration curve created by averaging the results obtained with short Carbon Nanotubes (short-cnts) and long Carbon Nanotubes (long-cnts).

4. CHAPTER 4: FINAL CONCLUSIONS

4.1. CONCLUSIONS ON RESULTS OBTAINED

This thesis discusses the development of an integrated system as a tool for the automated detection of a biological analyte with health and environmental safety implications.

The work has been performed during my internship at CNR NANOTEC in Lecce taking advantage of biological and chemistry facility, as well as of the opportunity to be in contact with real-world challenges commonly encountered during the laboratory activity. It includes, indeed, the realization of a system and user interface to simplify and improve the workflow of clinical operator. In particular, it automates a series of manual and time-consuming steps required to build an electrochemical biosensor measuring setup. The developed system integrates three key components, e.g. electrochemical measurement, microfluidics, and post-processing, which work cohesively and are involved in the development phase of the sensor. By automating these steps, the system allows clinical operators to organize and input the sequence of steps necessary for the development of the biosensor, which the system executes autonomously. This significantly optimizes the measurement process, reducing both manual effort and potential human error.

Tests performed on the electrochemical measurement component show that, the quantitative and qualitative analysis of the results obtained with the LabVIEW developed virtual instrument (VI) successfully replicates the outcomes obtained with NOVA as standard measurement setup. Minor differences that can be visually or numerically observed on the curves are likely due to the imperfect replicability of the measurements as well as the timing between consecutive measurements. On average, the variation between successive measurements is approximately 5%, which is within an acceptable range.

In addition, various algorithms for the post-processing of measurements were evaluated, thus achieving an optimal degree of reliability and automation on the calculation of the baseline from the DPV curves. This makes it possible to evaluate the entire measurement process, from start-up to saving the processed signal, fully automated and reliable.

Microfluidics control was successfully implemented. Micropumps were used as an additional mechanics to automate the development process of a biosensor, thus solution flow cycles can be

controlled. Indeed, cycles of washing, deposition, and placement of a redox couple drop for measurement are frequent during the development process. In a normal development environment, this may also require the user to temporarily remove the flat (working) electrode from the measurement set-up, which is a time-consuming process and requires high precision. The use of the implemented integrated system involves no need to remove the electrode, but the system of micro-tubes, connected to four micro-pumps, inserts and removes solutions directly on the surface of the working electrode.

Furthermore, it is shown that it is possible to integrate several devices to have a single system. This is controlled via an application created in LabVIEW, through which it is possible to control the system in its entirety, as well as its individual components. The innovativeness lies not in the individual components, but in the possibility to use the device to successfully automate the operation of the individual components and thus to pre-program the synthesis and test phases of an electrochemical biosensor. Finally, the VI operates correctly, providing automation and control for electrochemical measurements and microfluidics.

A MIP for cyromazine detection was therefore realized, the entire development process was followed using both the integrated system and the NOVA software, further demonstrating the correct reproducibility of the results obtained with the test program.

Furthermore, the use of the software in LabVIEW shows that it is possible to program and follow the entire development process, which takes place automatically. This allows development to proceed more quickly and, considering the proper functioning of the integrated system, minimizing human error during the process. this allows users to focus on other activities during the biosensor development process or for example the development could be performed at night after the user has set the sequence of operations. As part of “industrial series development plan” this approach allows the production of numerous highly specific biosensors. In a broader development context, this allows for point-of-care (POC) testing. In fact, the large number of highly specific biosensors. These low-cost biosensors can be used for rapid, on-site testing performing immediate results.

A 3D-printed chamber connected with electrodes and micropumps can also be developed, simplifying the integration of components into a cohesive macrosystem. This paves the way to develop a system that, considering the small scale of the individual components, is relatively easy to transport, once the device has been made as compact as possible.

4.2. FUTURE DEVELOPMENTS

The success of this thesis opens up numerous possibilities for future work. In the technological realm, the demonstration of the project's feasibility enables the integration of additional instruments at the hardware level. For instance, a multiplexer, could be introduced to enable sequential measurements on several connected devices. The switch would be controllable at the main interface level in LabVIEW, expanding the capability for high-throughput testing.

The system realized here allows for a large number of measurements to be performed in a short time without requiring the user presence. As that the system automatically saves the measurements in an orderly and methodical manner, a large number of measurements would then be available and properly classified. The large dataset generated could be utilized to realize machine learning models such as neural networks or pattern recognition algorithms.

This opens up a range of applications, including of medical diagnostics. One promising direction is the detection of TDP43, a Cytoplasmic aggregation of TAR DNA-binding protein 43, linked to neurodegenerative diseases like amyotrophic lateral sclerosis (ALS). At CNR Nanotec, it was possible to assess the concentration of this substance electrochemically, but tests on patient samples showed interference from other substances, making the detection difficult. This led to the idea of identifying a series of biomarkers whose presence could be linked to TDP43. This requires extensive of data from measurements at different TDP43 concentrations and known biomarkers. Once a set of adequately correlating biomarkers is identified, it would then be possible to integrate the dataset and thus estimate the TDP43 concentration indirectly by assessing the concentration of related biomarkers.

Moreover, advanced algorithms could be applied to signals pattern recognition, enabling the system to filter noise components or to distinguish between multiple signal components in complex electrochemical measurement. This development would extend the capability of the system increasing the applicability to a scientific and industrial fields.

BIBLIOGRAPHY

[1] "CNR Nanotec @ Lecce," [Online]. Available: https://nanotec.cnr.it/it/lecce.

[2] "oxidation-reduction-reaction," [Online]. Available: https://www.britannica.com/science/oxidation-reduction-reaction.

[3] L. Chemistry, "Voltaic Cells," [Online]. Available: https://chem.libretexts.org/Bookshelves/General_Chemistry/Map%3A_Chemistry_-_The_Central_Science_(Brown_et_al.)/20%3A_Electrochemistry/20.03%3A_Voltaic_Cells.

[4] D. G. Shamsher Singh, "Voltaic Cell," LibreTexts Chemistry, [Online]. Available: https://chem.libretexts.org/Bookshelves/Analytical_Chemistry/Supplemental_Modules_(Analytical_Chemistry)/Electrochemistry/Voltaic_Cells.

[5] H.-L. X. Y.-T. L. Xin Hua, "Revisiting a classical redox process on a gold electrode by operando ToF-SIMS: where does the gold go?," *Chemical Science,* 2019.

[6] E. P. K. B. M. Sijo Francis, "Electroanalytical techniques: a tool for nanomaterial characterization," *Elsevier,* pp. 163-175, 2022.

[7] A. Paccagnella, "Voltammetry and Amperometry, Biosensors," Padova.

[8] M. X. F.R. Simões, "Electrochemical Sensors," *Nanoscience and its Applications,* 2017.

[9] M. L. Vermereen V., "Evolution Towards the Implementation of Point-Of-Care Biosensors," *Biosensors for Health, Environment and Biosecurity,* 2011.

[10] M. R. V. J. R. E. Grieshaber D, "Electrochemical Biosensors - Sensor Principles and Architecture," *Sensors (Basel),* 2008.

[11] A. W. Y. L. J. J. X. J. H. Y. J. L. Sihua Peng, "Technology for Rapid Detection of Cyromazine Residues in Fruits and Vegetables: Molecularly Imprinted Electrochemical Sensors," *biosensors,* 2022.

[12] M. S. C. F. F. A. T. L. V. M. A. S. M. E. G. G. E. P. Giulia Siciliano, "Development of an MIP based electrochemical sensor for TGF-β1 detection and its application in liquid biopsy," *Analyst,* vol. 18, 2023.

[13] G. S. A. S. B. M. V. L. A. S. G. G. A. T. I. R. V. M. E. P. S. R. Gianluigi Zito, "Molecularly Imprinted Polymer Sensor Empowered by Bound States in the Continuum for Selective Trace-Detection of TGF-beta," *Advanced Science,* 2024.

[14] B. T. E. C. G.-C. A. P. S. Ahmad OS, "Molecularly Imprinted Polymers in Elecrochemical and Optical Sensors," *Trends Biotechnol,* 2019.

[15] j. J. G. Z. C. Chuang Peng, "A comparative study on electrochemical co-deposition and capacitance of composite films of conductiong polymers and carbon nanotubes," *ScienceDirect,* 2007.

[16] "LabVIEW," Wikipedia, [Online]. Available: https://it.wikipedia.org/wiki/LabVIEW.

[17] "LabVIEW - NI," [Online]. Available: https://www.ni.com/en/support/downloads/software-products/download.labview.html#521715.

[18] Bartels, "mp6 micropumps for liquids and gases," [Online]. Available: https://www.bartels-mikrotechnik.de/en/micropumps/.

[19] "Philips," [Online]. Available: https://www.philips.it/.

[20] "Operating Manual for the Micropump Driver mp6-QuadOEM".

[21] [Online]. Available: https://www.metrohm.com/it_it/products/a/ut20/aut204_s.html.

[22] "Nova_2.1_User_Manual".

[23] Metrohm, 1.11, Autolab SDK User Manual.

[24] F. C. M. J. Lukasz Gòrski, "Automatic baseline correction in voltammetry," *Elsevier,* 2014.

[25] B. W. A. T. Xiao-Jun Tang, "Baseline corection for infrared spectra using adaptive smoothness parameter penalized least squares method," *Spectrscopy Letters,* 2020.

ACKNOWLEDGEMENTS

My first thanks go to my lecturer, Professor Alessandro Paccagnella. Following a seminar at STMicrolectronics, he accepted my thesis proposal made well ahead of time (when I still lacked several exams) and offered to get in touch with CNR Nanotec in Lecce and supervise the work done while still leaving sufficient freedom to my internship tutor in choosing the direction of the work. I therefore thank my mentor, Dr. Francesco Ferrara, and Dr. Mariaserena Chiriacò for agreeing to get in touch with me (also well in advance of the canonical time frame), including me in their research group that they coordinate, and supervising my work. Thanks also to Dr. Lorenzo Dominici for the training in LabVIEW without which I would not have been able to realize the application presented in this thesis. Thanks also to Dr. Giulia Siciliano for supervising the measurement and testing part of the application and for having me work alongside her in the *cyromazine* detection study. Thank you to Drs. Valeria Garzanelli and Alessia Foscarini for allowing me to work alongside them in their experiments on wound healing, not mentioned in this thesis but a parallel work. Finally, an overall thank you to the entire research group team for welcoming me and integrating me into a healthy and happy working atmosphere. As I conclude this thesis, I do not know what exactly I will do but I hope to continue working with you in the period ahead.